FISEVIER

Contents lists available at ScienceDirect

Chemical Geology

journal homepage: www.elsevier.com/locate/chemgeo



Nitrogen diffusion in silicate minerals, with implications for nitrogen transport and cycling in the lithosphere



E.B. Watson^{a,*}, D.J. Cherniak^a, M. Drexler^a, R.L. Hervig^b, M.F. Schaller^a

- ^a Dept. of Earth and Environmental Sciences, Rensselaer Polytechnic Institute, Troy, NY 12180, USA
- ^b School of Earth and Space Exploration, Arizona State University, Tempe, AZ 85281, USA

ARTICLE INFO

Editor: Donald Porcelli

Keywords:
Nitrogen diffusion
Nitrogen in silicates
Nitrogen transport
Nitrogen cycling
Nitrogen in lithosphere
Nitrogen solubility

ABSTRACT

Diffusion laws for nitrogen in orthoclase, quartz, olivine and clinopyroxene were determined using a combination of experimental strategies that included: in-diffusion from C-H-O-N vapor; in-diffusion from molten NH₄Cl; and ion implantation followed by heating to mobilize N. Most experiments were conducted at pressures near 1 bar, but seven experiments were also run in a piston-cylinder device at $P_{\text{total}} = 1$ GPa. The C-H-O-N-source experiments were "wet" (H₂O present); those on ion-implanted samples were dry. All N sources were highly enriched in ¹⁵N to avoid spurious ¹⁴N signals resulting from surface contamination. Use of ¹⁵N also enabled depth profiling by nuclear reaction analysis (NRA) using the ¹⁵N(p, α Y)¹²C reaction, which has a detection limit of ~10 ppm. Nitrogen profiles in three samples were characterized by both NRA and SIMS, with similar results. A total of 17 to 28 diffusion coefficient measurements were made on each of the four minerals (83 in all), yielding results that conform for each mineral to an Arrhenius relation of the form $D = D_0 \exp(-E_a/RT)$. The following values for the pre-exponential constant (D_0) and activation energy (E_a) were obtained:

Mineral	$log(D_0, m^2/s)$	E _a (kJ/mol)	T range (°C)	
Orthoclase	-13.9 ± 0.4	95.4 ± 6.6	500-900	
Quartz	-12.4 ± 0.3	147.3 ± 5.7	550-1150	
Olivine	-14.2 ± 0.3	135.2 ± 6.6	650-1400	
Clinopyroxene	-14.1 ± 0.3	135.6 ± 7.4	750-1300	

The various experimental strategies yield generally indistinguishable results at a given temperature, and no significant effects of total pressure or $\rm H_2O$ are discernible in the overall diffusion data set. Experiments that involved in-diffusion from external N sources provide qualitative insight into the compatibility of N in the structures of the four minerals. Nitrogen concentrations attain the highest levels in orthoclase ($\sim 100-8000$ ppm atomic), with quartz, olivine and clinopyroxene falling in the tens to hundreds of ppm range. The new diffusion laws enable us to model the diffusive release of N acquired at depth in the crust during fluid-absent exhumation and cooling. In general, orthoclase is the least retentive of the minerals investigated, and will lose most of its N during cooling from $600\,^{\circ}$ C at tectonically typical rates. Olivine and clinopyroxene are the most retentive of N. Quartz is intermediate in retentivity between the mafic minerals and feldspar, but in all cases the extent of N exchange with the surroundings depends critically on the specific t-T path of the mineral of interest. In subduction settings where N-bearing fluid is released to the mantle wedge, diffusion is sufficiently fast to homogenize individual mafic mineral grains with respect to N over geologically plausible time scales, but equilibration on the outcrop or regional scale via volume diffusion is precluded by our data.

1. Introduction

Given the dominance of nitrogen in Earth's atmosphere and its

crucial role in biochemistry, the geochemical significance of this element is difficult to overstate. Nitrogen in the biosphere and soils and interactions with the atmosphere have been the subject of intensive

E-mail address: watsoe@rpi.edu (E.B. Watson).

^{*} Corresponding author.

investigation for many decades (see, e.g., Galloway, 2005; Bebout et al., 2013), but the potential importance of N in solid Earth was not widely appreciated until more recently. Investigations of terrestrial N have expanded to include studies of N speciation in deep-seated fluids (Brandes et al., 2008; Busigny and Bebout, 2013; Li and Keppler, 2014; Mikhail and Sverjensky, 2014; Mikhail et al., 2017), N solubility in minerals and mineral/fluid partitioning (Li et al., 2013, 2015), high P-T solubility of N in molten metals and silicates (Mysen et al., 2008; Mysen and Fogel, 2010; Roskosz et al., 2013); large-scale N storage and cycling models (Boyd, 2001; Busigny et al., 2003; Marty and Dauphas, 2003; Sadofsky and Bebout, 2004; Goldblatt et al., 2009; Mitchell et al., 2010; Busigny et al., 2011; Palva et al., 2011; Bebout et al., 2013; Cartigny and Marty, 2013; Johnson and Goldblatt, 2015, 2018; Houlton et al., 2018), and N concentrations and isotopic character of rock-forming minerals (e.g., Haendel et al., 1986; Bebout and Fogel, 1992; Bebout et al., 1999; Holloway and Dahlgren, 2002; Busigny et al., 2003; Li et al., 2007; Watenphul et al., 2010; Busigny et al., 2011). Despite this collective effort, significant gaps remain in our knowledge of N behavior in the solid Earth, in particular regarding interaction with major, ubiquitous rock-forming minerals. An especially glaring gap in our knowledge concerns N diffusion behavior in minerals that host relatively small concentrations of N but whose abundance in the lithosphere make them potentially significant reservoirs of terrestrial N (Holloway and Dahlgren, 2002; Johnson and Goldblatt, 2015; Houlton et al., 2018). To our knowledge, no data for N diffusion have been published for minerals other than diamond (see Jones et al., 2015; note, however, that N diffusion in Fe alloys has been well studied in metallurgy). This gap in knowledge is significant because volume diffusion in minerals might play a critical role in N uptake into (or loss from) volumetrically dominant crustal minerals, and in dispersal of subducted N in the mantle via diffusion in olivine and pyroxenes.

Volatile species in the atmosphere, biosphere and solid earth are inextricably linked over geologic time, but comprehensive characterization of nitrogen-mineral equilibria and kinetic properties is needed before these linkages can be fully understood for this important element. Here we focus on experimental characterization of N diffusion, targeting the major silicate minerals potassium feldspar (orthoclase), quartz, olivine, and clinopyroxene (a separate paper addresses calcite as an important host of N-bearing fluid inclusions that may represent ancient atmospheres; see Cherniak et al., 2018a). Some of our diffusion experiments involve N uptake from contacting fluid or vapor, so we also gain qualitative insight into mineral/fluid partitioning for specific cases.

2. Materials and methods

2.1. Overview

In studies of noble-gas diffusion, molecular speciation is not an issue, so in-diffusion experiments can be conducted simply by exposing the mineral of interest to a noble-gas atmosphere. The situation is more complicated in the case of N because geologically realistic systems contain elements (H, O) with which N can form polyatomic molecules or complex ions whose identities depend upon oxygen fugacity, pH and other intensive variables (e.g., Mikhail et al., 2017). "Soaking" of minerals in pure N2 gas would be a straightforward experiment, but also possibly lacking in desired realism. The present study included a number of experiments on geochemically realistic systems, but additional strategies were implemented to test the sensitivity of diffusion behavior to different methods of N introduction in minerals, and also to provide effective diffusion reversals. Our most realistic experiments involve exposure of the silicate minerals to f_{O2} -buffered C-H-O-N vapor or fluid produced by thermal decomposition of an amino acid, followed by depth-profiling the N uptake gradient. These experiments were performed in silica-glass ampoules at near-atmospheric pressure, and also in Ag capsules in a piston cylinder device. In the case of potassium

feldspar, most experiments involved diffusive uptake from molten NH_4Cl , where $K^+ \leftrightarrow NH_4^+$ exchange might be expected because of the similarity in ionic radius of the two ions (Sidey, 2016; see also Svensen et al., 2008 and Watenphul et al., 2009). A third type of experiment implemented for all four minerals was ion implantation followed by heating to mobilize N and depth profiling the resulting "relaxed" concentration profile. Altogether, 83 successful experiments were performed and analyzed, 32 of which involved in-diffusion from C-H-O-N vapor or molten NH₄Cl. Most of the results for clinopyroxene are from ion-implantation experiments, because this mineral tended to be heavily etched by C-H-O-N vapor at the high temperatures needed to mobilize N, which precluded acquisition of meaningful uptake profiles. The multiple-method strategy insured that diffusivities were obtained from experimental configurations that included differing initial and boundary conditions in the diffusion model used to fit the data, which is important in confirming that the resulting diffusivities do not depend on experiment design. At the same time, the multiple-method approach provided diffusion data for both nominally dry and wet conditions (ion implantation and C-H-O-N vapor experiments, respectively). All experiments on olivine and clinopyroxene—as well as all low-pressure C-H-O-N experiments in general—were f_{O2} -buffered.

To avoid potential complications arising from "environmental" nitrogen, all experiments were conducted using sources that were highly enriched in the rare isotope ^{15}N (0.364% of all N). The amino acids and ammonium chloride (both from Sigma Aldrich) contained 98% and 60–80% ^{15}N , respectively. In addition to circumventing possible adsorption/contamination issues, this strategy enabled depth-profiling of our experimental samples using the highly favorable $^{15}N(p,\alpha\gamma)^{12}C$ nuclear reaction, which gives a detection limit of $\sim\!10$ ppm for typical acquisition times (see Section 2.5).

2.2. Samples and surface preparation

The minerals investigated in this study were San Carlos olivine (Fo $_{90}$), optically clear synthetic quartz, Madagascar orthoclase, and natural diopside from De Kalb Township in St. Lawrence County, New York, U.S.A. One experiment was also run with augite from Templeton, Ontario (see Richter et al., 2014 for analyses of the clinopyroxenes). The silicates were prepared as oriented slabs cut with a low-speed diamond saw and polished using a sequential procedure ending with 2–4 h of automated polishing with colloidal silica. This is a standardized procedure in the RPI lab that has been demonstrated to result in a polished end-product that is free of near-surface structural damage (cracks, dislocations, etc.) that may have been introduced early in the cutting and polishing process (E.B. Watson et al., 2016). Quartz samples were cut both perpendicular and parallel to the c crystallographic axis; the feldspars, pyroxenes and olivines were cut parallel to the b axis.

2.3. Experiments with amino acid-derived vapor as the N source

A particular challenge in our in-diffusion experiments was the development of a geochemically realistic $^{15}{\rm N}$ source that is also affordable. In lieu of building a costly gas mixing/recycling system, we created C-H-O-N micro-environments through thermal decomposition of organic molecules in closed containers. Nitrogen-15 labeled amino acids are relatively affordable because of demand in bioscience research, and can be selected to yield geochemically plausible mixed-vapor compositions. When heated to temperatures in excess $\sim\!300\,^{\circ}{\rm C}$, amino acids decompose into much simpler molecules (Weiss et al., 2018), creating a mixed-volatile, external $^{15}{\rm N}$ diffusion source for any minerals present in the system. These experiments were performed both at near-atmospheric pressure in silica-glass ampoules and at 1 GPa in a piston-cylinder device.

Diffusion experiments conducted at low pressure in glass ampoules were prepared by placing a carefully weighed mass of amino acid (aminobutyric acid $[C_4H_9^{15}NO_2]$ or glycine $[C_2H_5^{15}NO_2]$) in the

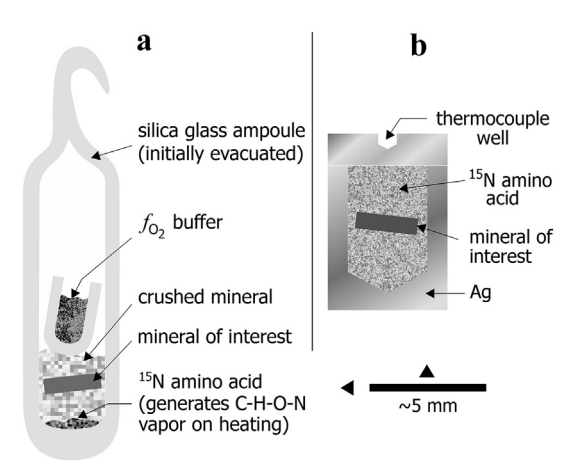


Fig. 1. Configurations of experiments involving diffusive uptake (in-diffusion) of nitrogen into minerals. The total pressure of the C-H-O-N vapor in the silica glass ampoules (a) is believed to have been < 10 bars based on the mass of 15 N-labeled amino acid vapor source and the strength of the glass. Note that a similar set up was used for in-diffusion experiments using a molten 15 NH₄Cl source, but in that case no oxygen buffer was included in the ampoule. The configuration in (b) was used for piston-cylinder experiments conducted at 1 GPa.

bottom of a silica glass tube (typically 6 mm I.D. × 8 mm O.D.) that had been closed at one end with an H₂-O₂ or oxy-acetylene torch. A coarse powder of the mineral of interest was placed on top of the amino acid, followed by the polished sample under study ($\sim 3 \times 3 \times 1$ mm), more mineral powder, and, lastly, an open silica-glass cup containing a solid oxygen buffer (Ni-NiO). The silica tube was then evacuated and the assembly (amino acid + sample + buffer) sealed off with a torch and detached from the tube (Fig. 1a). The resulting evacuated glass ampoule was suspended vertically in a tube furnace at a predetermined temperature (500°-950 °C) for durations of \sim 0.2 to 25 days. This technique was uniformly successful at temperatures below 900 °C, but higher temperatures were generally precluded because the hydrous vapor etched the mineral surfaces, making it unsuitable for depth profiling. Experiments were terminated by pulling the glass ampoules out of the vertical furnace and allowing them to cool in air. The ampoules emerged intact in most cases, making an audible pop when broken with a hammer to recover the diffusion sample. The solid-state buffers were recovered for confirmation that both Ni and NiO were still present and "unarmored". The inside surfaces of the silica glass ampoules were coated with a translucent layer of small cristobalite crystals ~10 µm in size. These crystals constitute evidence of silica mobilization, and confirm the presence of H₂O in the vapor (silica minerals are not appreciably soluble in CO₂ or N₂).

For several reasons, the molecular composition of the C-H-O-N atmospheres produced by decomposition of amino acids is not exactly known, but meaningful estimates can be made. The C:H:O:N elemental proportions—2:5:2:1 for glycine and 4:9:2:1 for aminobutyric acid—are clearly hydrogen-rich, and closed-system decomposition in the absence of an oxygen buffer would yield a vapor dominated by reduced molecular species. However, the presence of the Ni-NiO buffer in our sealed ampoules changes the molecular speciation dramatically: qualitative equilibrium calculations predict a vapor composition dominated by ${\rm CO}_2$, ${\rm H}_2{\rm O}$ and ${\rm N}_2$, with diminishingly small mole fractions of reduced species NH₃ and H₂ ($\sim 10^{-15}$ and 10^{-8} , respectively, at 800 °C). The calculations cannot be quantified with confidence because the total pressure is not precisely known, and also because the ampoules are unlikely to remain a completely closed system due to diffusive loss of some molecular species into or through the glass (H2 and H2O, in particular). From the standpoint of the diffusion experiments, the key knowledge is that the dominant C- and H-bearing molecular species are oxides, and that N exists as N2 not NH3. Importantly, diffusivities

extracted from in-diffusion experiments are not sensitive to the surface concentration of the diffusant, or even to modest changes in the surface concentration during the course of an experiment. Ultimately, the value of the diffusivity depends mainly on penetration depth.

High-pressure experiments in which aminobutyric acid or glycine served as the 15 N source were conducted at \sim 1 GPa in a piston-cylinder device in thick-walled Ag containers. Prior to an experiment, the polished mineral sample of interest was packed in the Ag container with amino acid and covered with a pressure-sealing lid (Fig. 1b). Upon opening the container after an experiment, the sample was usually found resting on the bottom, encased in soft graphitic material, with liquid $\rm H_2O$ visible at the top in most cases. No oxygen buffer was used in the piston-cylinder experiments, but the presence of graphite in the run products (from breakdown of amino acid accompanied by bulk hydrogen loss) indicates oxygen fugacities near the graphite-CO-CO₂ buffer (the identity of the graphite was confirmed by Raman spectroscopy).

2.4. Experiments on orthoclase using NH₄Cl as the N source

Ammonium ions are known to substitute for K+ in K-bearing minerals such as micas and K-feldspar (e.g., Honma and Itihara, 1981; Duit et al., 1986). For this reason, the majority of ¹⁵N diffusion experiments on orthoclase were set up in a manner designed to promote NH₄⁺ ↔ K⁺ exchange between feldspar and diffusion source—specifically by immersion of feldspar samples in molten 15NH4Cl (m.p. = 338 °C; B.P. = 520 °C). Most of these experiments were conducted in evacuated silica-glass ampoules using procedures similar to those employed for the low-pressure C-H-O-N source experiments on other minerals, but lacking the oxygen buffer. A single experiment was conducted on orthoclase with the molten NH₄Cl source in an Ag capsule at 1 GPa. The NH₄ + exchange experiments on orthoclase were complemented with additional runs using the decomposed amino acid ¹⁵N source (in this case ¹⁵N glycine), and three additional measurements were carried out by implanting the samples with 100-keV N+ ions and holding then at high temperature for predetermined durations to mobilize the nitrogen (next section).

2.5. Ion implantation experiments

Ion implantation is an effective way to introduce diffusants into solids, provided it can be demonstrated that any damage to the crystal structure associated with the stopping of high-energy ions does not affect subsequent diffusion measurements. In cases where significant damage does occur during implantation, heating of the sample can activate competing kinetic phenomena-i.e., annealing (repair) of the damage and diffusion of the implanted species-that might hinder recovery of accurate diffusion data. In general, low-mass implants tend to cause minor damage in the target mineral, with few atom displacements (e.g., Nastasi et al., 1996). However, different minerals respond in different ways to energetic ion beams (zircon, for example is more prone to structural damage from energetic particles than most other minerals; see Ewing et al., 1995; Wang et al., 1999). Diffusion measurements made on ion-implanted materials have been shown to agree very well with measurements made by introducing diffusants in other ways (e.g., Cherniak et al., 2014; Trail et al., 2016). Ion implantation can thus serve as a complement to in-diffusion experiments (or vice versa), and agreement between the results of the two approaches is a strong validation of both. Ion implantation can, in addition, circumvent problems of interface reaction at high temperatures between minerals and surface sources of diffusants. This advantage allowed us to extend our N diffusion measurements on clinopyroxene and San Carlos olivine to 1300 °C and 1400 °C, respectively, where the moist C-H-O-N vapor source chemically attacked the mineral surfaces. In the cases of quartz and orthoclase, ion implantation measurements were used as a complement to results from in-diffusion runs.

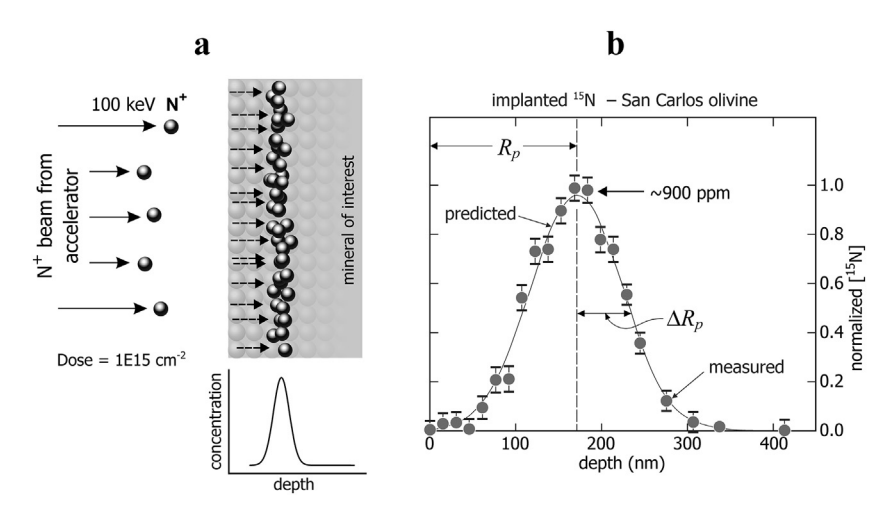


Fig. 2. Illustration of N $^+$ implantation, including a schematic of the phenomenon itself (a) and the resulting distribution of 15 N in the sample (b). The graph includes the profile predicted by the SRIM program (Ziegler and Biersack, 2006; continuous curve) and that measured by nuclear reaction analysis (gray circles). R_p is referred to as the *ion range*; Δ R_p is the *range straggle*. See text for more details.

For the implantation experiments, samples were cut and polished as described in Section 2.2 and mounted on an aluminum plate for implantation with 100 keV $^{15}\mathrm{N}^{+},$ produced in the Extrion ion implanter at the Ion Beam Laboratory at the University at Albany (Fig. 2a). Implant doses were $1 \times 10^{15} \,\mathrm{N}\,\mathrm{atoms/cm^2}$. The resulting implantation profile is close to a Gaussian distribution of 15N atoms centered at a depth (or range, R_p) of ~180 nm and having a range straggle, ΔR_p , of ~65 nm (see Fig. 2b; both distances depend slightly on the target material). At the dose used in this study, the concentration of ¹⁵N at the peak of the Gaussian was approximately 900 ppm atomic (see Fig. 2b). After implantation, samples were removed from the aluminum plate and cleaned with ethanol in an ultrasonic bath. Diffusion anneals lasting ~0.014 to 25 days at temperatures ranging from 500° to 1400 °C were conducted on the implanted materials. This heat treatment mobilized the ¹⁵N and resulted in relaxation of the implanted Gaussian profiles to varying degrees, depending on sample identity, annealing duration and temperature. The diffusion anneals involving San Carlos olivine and natural clinopyroxene were conducted at near-atmospheric pressure in evacuated silica-glass ampoules under oxygen-buffered conditions (Ni-NiO except for one experiment at iron-wüstite). Nitrogen-implanted quartz and orthoclase samples were annealed in air.

2.6. Confirming experiments: time series and "reversal"

Whenever possible, a rigorous experimental study of diffusion should include a demonstration that the diffusivities extracted from the profiled samples run at a given temperature do not depend on experiment duration. For each of the minerals examined in this study, we included a time series of four or five experiments conducted at the same temperature but with durations varying by a factor of at least ~5 and in most cases a factor of ~10. Large time differences are highly desirable because of the square-root dependence of diffusion distance upon time—but there are the practical limitations: for long durations the limitation is to available furnace time and the desired time frame for completion of a study; for short durations the limitation involves the accuracy with which a concentration profile can be characterized given the 5-10-nm depth resolution of NRA. In the case of orthoclase, the time series consisted of 4 in-diffusion experiments (3 with the NH₄Cl source; 1 with the C-H-O-N vapor source) and one implantation anneal, all at 700-710 °C. For the other minerals, the time series involved relaxation of implantation profiles for 4 different durations (olivine and clinopyroxene at 1100 °C, quartz at 800 °C) plus one extended C-H-O-N in-diffusion result for quartz.

An additional procedure for confirming expected diffusion behavior is to effectively reverse the diffusant flux: N diffused into a mineral at high temperature from an external source should diffuse out when the external source is removed and the sample returned to high

temperature. This confirmation was conducted on a San Carlos olivine sample into which N was diffused at 850 °C and 1 GPa for \sim 3 days, generating an in-diffusion profile \sim 150 nm in length (experiment no. N-3). The sample was recovered from the piston-cylinder device, profiled by NRA, and returned to high temperature (800 °C) for \sim 1 day in an evacuated silica glass ampoule with a Ni-NiO oxygen buffer. Re-analysis of the sample by NRA should reveal partial loss of N by out-diffusion at a rate consistent with the diffusion data collected from other types of experiments (see Section 3.1).

2.7. Depth profiling with nuclear reaction analysis (NRA)

Both the in-diffusion experiments and those on ion-implanted samples were profiled using nuclear reaction analysis (NRA) at the Ion Beam Laboratory at the University at Albany. The specific nuclear reaction is $^{15}N(p,\alpha\gamma)^{12}C$, which some readers may recognize as the same one that has been used extensively to depth-profile H in minerals, glasses, and other condensed materials (e.g., Laursen and Lanford, 1978; Rossman et al., 1988; Hammer et al., 1996; Maldener et al., 2003; Bell et al., 2004). In the present case, the sample is bombarded with energetic protons, some of which engage in a reaction with the nuclei of ¹⁵N atoms introduced by in-diffusion or ion implantation [for H profiling, the situation is reversed: the beam is ¹⁵N⁺ ions and the target is ¹H nuclei in the sample, in which case the reaction is written ¹H $(^{15}\text{N},\alpha\gamma)^{12}\text{C}$]. The $^{15}\text{N}(p,\alpha\gamma)^{12}\text{C}$ reaction has a particularly high probability of occurring when the incident protons have a specific energy of 897 keV—i.e., it has a resonance at this energy. If the energy of the incident protons coincides with the resonance energy, the reaction with ¹⁵N will occur at the sample surface. If, on the other hand, the protons have an energy somewhat greater than the resonance energy, the reaction will occur at a depth in the sample where the protons have been slowed to the resonance energy (Fig. 3). The proton beam can thus be tuned, energy-wise, to detect ¹⁵N at a desired depth in the sample if the proton energy-loss characteristics of the host mineral are known. Counting the 4.43-MeV γ associated with the reaction quantifies [15 N] at a given depth. The favorable reaction cross-section for $^{15}N(p,\alpha\gamma)^{12}C$ results in a low detection limit of ~10 ppm (atomic), and the sharp resonance leads to a near-surface depth resolution of 5-10 nm.

2.8. Depth profiling by ion probe

Nuclear reaction analysis (NRA) is a well-established technique that is familiar to materials scientists (see, e.g., Jeynes and Colaux, 2016) but relatively unknown in geochemical circles. For this reason, our study included a subset of samples that were depth-profiled using both NRA and secondary ion mass spectrometry (SIMS), the latter performed in the SIMS laboratory at Arizona State University. In preparation for

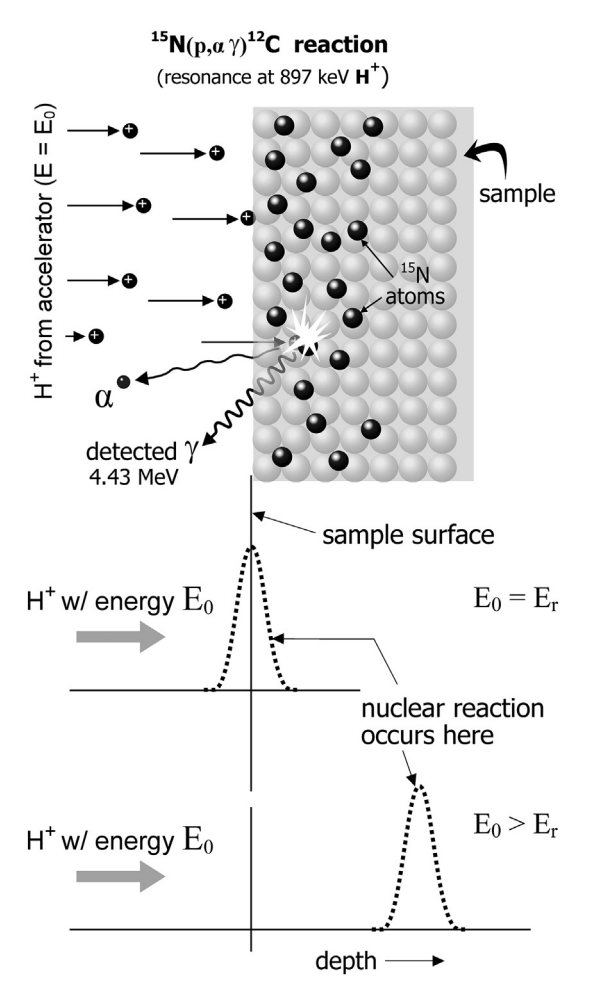


Fig. 3. Schematic illustration of nuclear reaction analysis (NRA) utilizing the 15 N(p, $\alpha\gamma$) 12 C reaction. See text for further description.

ion probe analysis, selected quartz and San Carlos olivine diffusion samples were pressed into indium with the target surface facing out and coated with ~20 nm of Au. Depth profiles were acquired using a primary beam of mass-filtered $^{16}\mathrm{O}^-$ extracted from a duoplasmatron held at -12,500 V, and detection of positive secondary ions accelerated to +5000 V. A primary current of 60 nA was used for profiling ¹⁵N-implanted silica and 90 nA for ¹⁵N-implanted and in-diffused olivine. The mass resolution (M/ Δ M at 10% of the peak height) was set at ~900, which will not completely separate interfering $^{30}\text{Si}^{++}$ from $^{15}\text{N}^{+}$. However, the ¹⁵N⁺ was a distinct, flat-topped shoulder adjacent to the doubly-charged silicon peak, minimizing contribution of Si⁺⁺ to the nitrogen ion signal. The depth profiling was conducted as described in Cherniak et al. (2010). Secondary ion intensities (integration times in parentheses) for $^{28}\mathrm{Si}^{++}$ (1 s), $^{14}\mathrm{N}^{+}$ (1 s) and $^{15}\mathrm{N}^{+}$ (10 s) were obtained in each cycle, and sample charging was alleviated by ramping the sample voltage (also in each cycle) from 4980 to 5080 V while monitoring the signal for ²⁸Si + + and returning the sample voltage to the centroid of the curve. The depth of the resulting crater ranged from 300 to 800 nm as determined by stylus profilometry, and is accurate to \pm 5%.

Because of the low ion yield for nitrogen as the positive ion (e.g., Regier et al., 2016), we attempted to increase the signal by maximizing the area within the crater from which secondary ions were allowed into the mass spectrometer (a circular area 75 μm in diameter). The raster size ranged from $125\times125\,\mu m^2$ to $175\times175\,\mu m^2$, but despite using the smaller raster, there was no evidence for any contribution of N ions from the crater walls to the signal.

Examination of the ²⁸Si ^{+ +} and N ⁺ signals in the implanted samples

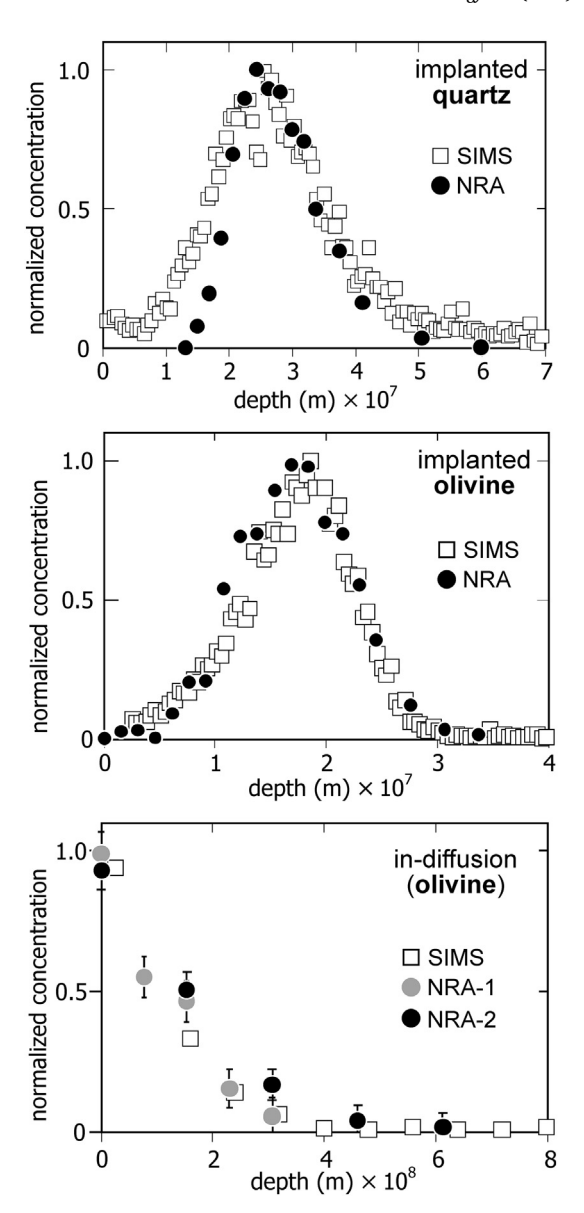


Fig. 4. Comparison of ¹⁵N depth profiles obtained by NRA (at UAlbany) and SIMS (at Arizona State University). The top two panels show implantation profiles in quartz and San Carlos olivine; the bottom panel compares a SIMS profile with two separate NRA profiles in San Carlos olivine.

showed: 1) the "transient regime" over which the chemistry of the crater floor is changing from its original composition to steady-state with the additional primary oxygen is approximately 100 nm; and 2) some nitrogen surface contamination was present with near normal nitrogen isotope ratios in the first ~20 nm of sputtering (presumably associated with surface contamination mingled with the ~20-nm Au coat). For both implanted and in-diffused ¹⁵N, the ion-probe depth profiles compare favorably with those obtained by NRA on the same quartz and olivine samples (Fig. 4).

2.9. Extraction of N diffusivities and qualitative partitioning information

Diffusion coefficients were obtained from in-diffusion profiles by fitting the concentration *vs.* depth data to the solution to the non-steady state diffusion equation (in 1 dimension) for diffusion into an infinite half-space with the surface concentration held constant:

$$\frac{C(x,t)}{C_o} = 1 - erf\left(\frac{x}{\sqrt{4Dt}}\right) \tag{1}$$

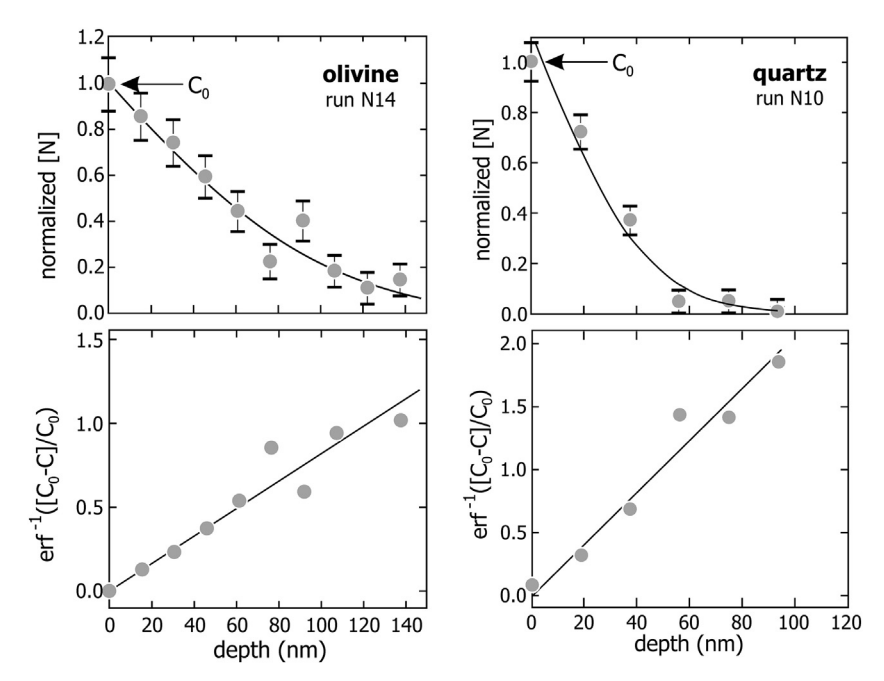


Fig. 5. Examples of ¹⁵N diffusive uptake profiles in quartz and San Carlos olivine (top panels) with linearized versions shown in the bottom panels. The diffusivities were calculated from the slopes of these lines, which equal $(4Dt)^{-\frac{1}{2}}$.

where C_o is the concentration at the surface, x is distance into the sample from the surface (at x = 0), t is experiment duration, and D is the diffusivity. Diffusivities were computed by plotting the data in linearized form—i.e., $erf^{-1}\left[\frac{C_0-C(x,t)}{C_0}\right]vs.$ *x*—fitting a line to the array, and computing *D* from the slope, which is $(4Dt)^{-1/2}$ (see example in Fig. 5). One or two iterations with adjusted estimates of C_0 were sometimes needed to obtain a line passing through the origin. In principle, C_o represents the equilibrium concentration in the diffusion sample coexisting with the diffusant source (see arrows in Fig. 5). For example, if the vapor source were pure N_2 , then C_o would be the solubility of N₂ at the conditions of the experiment. Because the gases or fluids produced by decomposition of amino acids contain other molecules besides N2, the surface concentration should reflect not the N solubility but rather the N partitioning equilibrium between the mineral and its surrounding vapor or fluid. We recorded these surface-intercept concentrations (C_0 values) to serve as qualitative guides to N uptake in silicate minerals from N2-bearing fluids, but we emphasize that these numbers must be regarded as rough approximations because of the uncertainties in the compositions of amino acid-derived gases and fluids

Diffusivities were obtained from the partially relaxed implantation profiles using a model that assumes an initial Gaussian distribution that relaxes over time according to:

$$C(x,t) = \frac{C_{\text{max}}}{2} \cdot \left(1 + \frac{2Dt}{\Delta R_p^2} \right)^{-1/2} \left\{ \exp\left[-\frac{(x - R_p)^2}{2\Delta R_p^2 + 4Dt} \right] \right.$$

$$\times \left[1 + erf\left(\frac{\frac{R_p \sqrt{4Dt}}{\Delta R_p \sqrt{2}} + \frac{x\Delta R_p \sqrt{2}}{\sqrt{4Dt}}}{\sqrt{2\Delta R_p^2 + 4Dt}} \right) \right] - \left. \exp\left[-\frac{(x + R_p)^2}{2\Delta R_p^2 + 4Dt} \right] \times \left[1 + erf\left(\frac{\frac{R_p \sqrt{4Dt}}{\Delta R_p \sqrt{2}} - \frac{x\Delta R_p \sqrt{2}}{\sqrt{4Dt}}}{\sqrt{2\Delta R_p^2 + 4Dt}} \right) \right] \right\}$$

$$(2)$$

where C_{max} is the maximum concentration of the implanted species (here ~900 ppm ¹⁵N), R_p is the depth in the sample (the range) where

the maximum implanted N concentration occurs, and ΔR_p is the range straggle, or half width at half maximum of the initial Gaussian (Ryssel and Ruge, 1986). Values for R_p and ΔR_p for ¹⁵N were obtained using the Monte Carlo simulation program SRIM 2006 (Ziegler and Biersack, 2006), and also confirmed by NRA (see Fig. 2).

3. Results and discussion

3.1. Diffusion systematics

Nitrogen diffusivities for orthoclase, quartz, olivine and clinopyroxene are plotted in Fig. 6 on Arrhenius-type diagrams, anticipating a log-linear dependence of the diffusivity D_N on absolute temperature $T(K)^{-1}$.

$$D_N = D_0 \exp\left[-\frac{E_a}{RT}\right] \tag{3}$$

where D_0 is the pre-exponential or frequency factor (in m²/s) and E_a is the activation energy for diffusion (in J/mol); the values of these Arrhenius parameters are shown on the figures. The individual diffusivities, with uncertainties, are summarized in Table 1. Some general observations follow.

Nitrogen diffusion in all four minerals is well-behaved in the sense that the measured diffusivities form linear arrays in $\log D$ vs. $T(K)^{-1}$ space (Fig. 6a–d), with most values falling on the best-fit lines within uncertainty. This is remarkable for several reasons, not least of which is that the data span a large temperature range (700°, 550° and 600°C, respectively, for olivine, clinopyroxene and quartz). The extensive coverage is advantageous because it means that the uncertainties in D_0 and E_a are minimized and that the data can be applied to natural systems of interest with little if any extrapolation in temperature. In the case of orthoclase, the experimental temperatures range from 500° to 900°C, encompassing the range appropriate for most geologic applications.

A particularly interesting characteristic of the diffusion data for all four minerals is that values obtained from in-diffusion experiments and from annealing of ion-implanted samples are generally consistent within error (for this reason, the two "types" of data are pooled to calculate Arrhenius parameters). In the case of olivine (Fig. 6d),

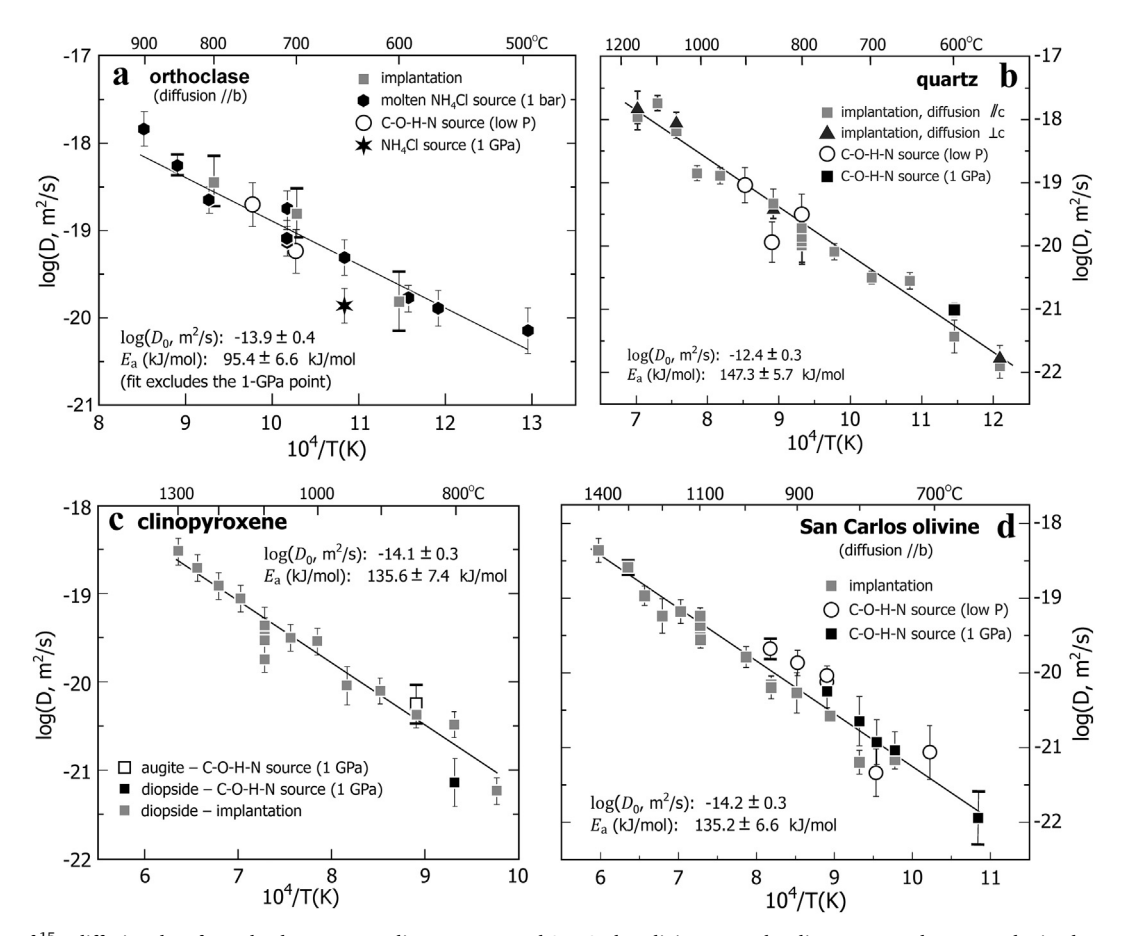


Fig. 6. Summary of 15 N diffusion data for orthoclase, quartz, clinopyroxene and San Carlos olivine. Most the clinopyroxene data were obtained on De Kalb diopside, with one result for Templeton augite. Note that the data were acquired using four different experimental methods, with broad agreement among results, indicating little if any dependence of the diffusivity on the presence of H_2O , the method of N introduction into the samples, or P_{total} . Uncertainties are \pm 1 standard deviation. See text for discussion.

diffusivities obtained from low-pressure in-diffusion experiments might be marginally higher than those recovered from ion-implantation experiments, but separate fits do not seem warranted. Nitrogen diffusion in quartz does not depend upon crystallographic orientation, inasmuch as the two measurements for diffusion $\perp c$ fall on the line for diffusion //c. In general, the results of "wet" in-diffusion experiments with the C-H-O-N source-at both low pressure and 1 GPa-do not differ significantly from the "dry" values obtained by ion implantation. The possible exception to this generalization is the single 1-GPa value obtained from the 1-GPa NH₄Cl-source experiment on orthoclase, which falls roughly 0.5 log units below the best-fit line. For orthoclase, the 1-GPa value is included in Fig. 6a but excluded from the best-fit Arrhenius line used for modeling. On the whole, however, it is clear that neither total pressure nor $P_{\rm H2O}$ in the system have marked effects on N diffusion in the silicates examined. Also noteworthy is the fact that the single datum for augite falls on the Arrhenius line for diopside, suggesting that N diffusion in clinopyroxene is not sensitive to major-element compo-

The results of the time series for each mineral are shown in Fig. 7, from which it is clear that the reported diffusivities are independent of experiment duration within the uncertainty of the measurements. In the case of orthoclase, the shorter-duration experiments (\sim 4 and 20 h), yielded slightly higher apparent diffusivities than the longer runs. This is not uncommon for in-diffusion results because short profiles challenge the \sim 10-nm spatial (depth) resolution of the analytical method, potentially leading to minor analytical spreading and slightly elevated diffusivities. The results of the "reversal" experiment on San Carlos olivine (experiment N-3R; Table 1) confirm that in-diffused N

(experiment N-3) can be induced to diffuse out when the source is removed, and that the two treatments yield diffusivities consistent with one another and with the rest of the data (Fig. 8).

3.2. Nitrogen speciation

The N diffusion results for orthoclase warrant additional discussion because this is the one mineral included in our study for which a welldocumented exchange mechanism (NH₄ $^+ \leftrightarrow$ K $^+$) could allow N to enter the crystal structure (e.g., Mookherjee et al., 2005). We had anticipated that immersion of orthoclase in molten NH_4Cl would result in 1:1 $N \leftrightarrow K$ exchange, with 4 protons accompanying each N. In general, the orthoclase took in more N than the other minerals (see Section 3.2), but the loss of K (measured by Rutherford backscattering spectroscopy) was greater than needed to balance the gain of N, assuming NH₄⁺ to be the in-diffusing species. In addition, the concentration of in-diffused H (measured by NRA; see Section 2.7) was much higher than $4 \times [N]$, implying that most of the exchange that occurred during these experiments involved $H^+ \leftrightarrow K^+$, not $NH_4^+ \leftrightarrow K^+$. The latter exchange cannot be ruled out on the basis of our data, but it seems to have contributed to K exchange in only a minor way. Given the good agreement of N diffusivities obtained using the NH₄Cl source with those obtained using both the C-H-O-N source and ion implantation, it seems likely that N enters the feldspar structure as more than one species: a minor fraction may be as NH₄⁺, but the diffusivity is the same whether or not K is involved. Note, also, that the position of our Arrhenius line for N diffusion in orthoclase relative to those for K and Rb is also difficult to reconcile with N diffusing as NH₄ ⁺ in orthoclase (Fig. 9). The result is

Table 1
Summary of nitrogen diffusion experiment parameters and results.

	_		. 1-	_	4				
Expt ID	Type ^a	T(C)	f_{02}^{b}	Bars ^c	Slab ^d	Time (s)	D (m ² /s)	logD	±
NOrth-14	NH ₄ Cl	499	na	~1	//(010)	6.84×10^{5}	7.17×10^{-21}	-20.14	0.1
xp-A	NH ₄ Cl	566	na	~1	//(010)	5.99×10^{5}	1.29×10^{-20}	-19.89	0.1
хр-В	NH ₄ Cl	591	na	~1	//(010)	1.73×10^{5}	1.64×10^{-20}	-19.78	0.1
хр-С	NH ₄ Cl	650	na	~1	//(010)	2.43×10^{5}	4.86×10^{-20}	-19.31	0.
xp-O	NH ₄ Cl	710	na	~1	//(010)	3.33×10^{5}	8.40×10^{-20}	-19.09	0.3
xp-L	NH ₄ Cl	710	na	~1	//(010)	7.56×10^{4}	1.76×10^{-19}	-18.75	0.
Orth-13	NH ₄ Cl	710	na	~1	//(010)	1.73×10^{5}	7.30×10^{-20}	-19.14	0.
xp-M	NH ₄ Cl	805	na	~1	//(010)	7.92×10^4	2.26×10^{-19}	-18.65	0.
Orth-12	NH ₄ Cl	850	na	~1	//(010)	1.98×10^{4}	5.60×10^{-19}	-18.25	0.
Orth-11	NH ₄ Cl	900	na	~1	//(010)	5.40×10^{3}	1.45×10^{-18}	-17.84	0.:
Orth-15	gly	750	NNO	< 10	//(010)	5.40×10^4	2.00×10^{-19}	-18.70	0.:
IOrth-16	gly	700	NNO	< 10	//(010)	1.37×10^{5}	5.75×10^{-20}	-19.24	0.:
xp 1 GPa	NH ₄ Cl	650	na	10^{4}	//(010)	3.46×10^{5}	1.37×10^{-20}	-19.86	0.
IimpOrth	impl	800	Air	1	//(010)	7.20×10^{3}	3.62×10^{-19}	-18.44	0.
limpOrth	impl	700	Air	1	//(010)	1.44×10^{4}	1.58×10^{-19}	-18.80	0.
limpOrth	impl	600	Air	1	//(010)	8.28×10^{4}	1.55×10^{-20}	-19.81	0.:
Quartz									
Expt ID	Type ^a	T(C)	f_{02}^{b}	Bars ^c	Slab ^d	Time (s)	D (m ² /s)	logD	±
NimpQtz-11	impl	554	Air	1	⊥c	1.13 × 10 ⁶	1.27×10^{-22}	-21.90	0.1
limpQtz-8	impl	600	Air	1	⊥c	5.90×10^5	3.70×10^{-22}	-21.43	0.:
IimpQtz-7	impl	650	Air	1	⊥c	2.30×10^{5}	2.82×10^{-21}	-20.55	0.
limpQtz-2	impl	698	Air	1	⊥c	4.88×10^{5}	3.15×10^{-21}	-20.50	0.
limpQtz-4	impl	750	Air	1	⊥c	1.80×10^{5}	8.17×10^{-21}	-20.09	0.
limpQtz-1	impl	800	Air	1	⊥c	9.54×10^4	1.90×10^{-20}	-19.72	0.
impQtz-18	impl	800	Air	1	⊥c	2.56×10^{5}	1.05×10^{-20}	-19.98	0.
impQtz-19	impl	800	Air	1	⊥c	2.34×10^{4}	1.21×10^{-20}	-19.92	0.
limpQtz-20	impl	800	Air	1	⊥c	1.08×10^{4}	1.41×10^{-20}	-19.85	0.
IimpQtz-9	impl	848	Air	1	⊥c	1.26×10^{4}	4.70×10^{-20}	-19.33	0.
limpQtz-5	impl	950	Air	1	⊥c	1.08×10^{4}	1.28×10^{-19}	-18.89	0.
limpQtz-6	impl	1000	Air	1	⊥c	5.40×10^{3}	1.40×10^{-19}	-18.85	0.
limpQtz-13	impl	1049	Air	1	⊥c	2.40×10^{3}	6.56×10^{-19}	-18.18	0.
limpQtz-15	impl	1099	Air	1	⊥c	1.80×10^{3}	1.83×10^{-18}	-17.74	0.
limpQtz-16	impl	1151	Air	1	⊥c	1.20×10^{3}	1.12×10^{-18}	-17.95	0.:
limpQtz-12	impl	554	Air	1	//c	1.13×10^{6}	1.71×10^{-22}	-21.77	0.
limpQtz-10	impl	848	Air	1	//c	1.26×10^{4}	3.68×10^{-20}	-19.43	0.
limpQtz-14	impl	1049	Air	1	//c	2.40×10^{3}	8.59×10^{-19}	-18.07	0.
IimpQtz-17	impl	1151	Air	1	//c	1.20×10^{3}	1.52×10^{-18}	-17.82	0.
I-10	abt	600	g	10^{4}	⊥c	6.05×10^{5}	9.71×10^{-22}	-21.01	0.
V-13	abt	800	NNO	< 10	⊥c	4.97×10^{5}	3.17×10^{-20}	-19.50	0.
V-15	abt	850	NNO	< 10	⊥c	4.07×10^{5}	1.14×10^{-20}	-19.94	0.:
N-17	abt	900	NNO	< 10	⊥c	5.99×10^{5}	9.19×10^{-20}	-19.04	0.:
San Carlos olivin	e								
Expt ID	Type ^a	T(C)	$f_{\mathrm{O2}}^{}\mathrm{b}}$	Bars ^c	Slab ^d	Time (s)	D (m ² /s)	logD	±
limpOl-8	impl	750	NNO	1	//(010)	1.81×10^{6}	6.72×10^{-22}	-21.17	0.0
impOl-0	impl	800	NNO	1	//(010)	7.92×10^{5}	6.72×10^{-22} 6.32×10^{-22}	-21.17	0.
impOl-1	impl	845	NNO	1	//(010)	4.10×10^{5}	2.60×10^{-21}	-20.58	0.
impOl-4	impl	901	NNO	1	//(010)	2.66×10^{5}	5.40×10^{-21}	-20.27	0.
impOl-9	impl	948	NNO	1	//(010)	2.76×10^{5}	6.92×10^{-21}	-20.16	0.
impOl-3	impl	948	IW	1	//(010)	1.48×10^{5}	6.32×10^{-21}	-20.10	0.
impOl-11	impl	998	NNO	1	//(010)	8.28×10^4	1.64×10^{-20}	-19.79	0.
impOl-10	impl	1100	NNO	1	//(010)	3.06×10^4	2.76×10^{-20}	- 19.79 - 19.56	0.
impOl-5 impOl-12	impl	1100	NNO	1		1.44×10^4	3.97×10^{-20}	-19.40	0.
impOl-12 impOl-13	•	1101	NNO		//(010)	7.56×10^4	3.97×10^{-20} 4.27×10^{-20}	- 19.40 - 19.37	0.
•	impl impl	1101	NNO	1 1	//(010)	1.51×10^{5}	4.27×10^{-20} 5.80×10^{-20}	- 19.37 - 19.24	0.
impOl-14	impl impl				//(010)	1.51×10^{4} 1.98×10^{4}	6.62×10^{-20}		
limpOl-6	impl	1150	NNO	1	//(010)			-19.18	0.
limpOl-3	impl	1199	NNO	1	//(010)	1.44×10^4	5.79×10^{-20}	-19.24	0.
limpOl-15	impl	1250	NNO	1	//(010)	1.08×10^4	1.07×10^{-19}	-18.97	0.
limpOl-2	impl	1300	NNO	1	//(010)	7.20×10^3	2.59×10^{-19}	-18.59	0.
limpOl-16	impl	1401	NNO	1	//(010)	3.60×10^{3}	4.40×10^{-19}	-18.36	0.
I-5	abt	650	g	10 ⁴	//(010)	2.16×10^{6}	1.11×10^{-22}	-21.95	0.
V-12	abt	705	NNO	< 10	//(010)	4.32×10^{5}	8.64×10^{-22}	-21.07	0.
1-2	abt	750	g	10 ⁴	//(010)	5.78×10^{5}	9.08×10^{-22}	-21.04	0.
	abt	775	σ.	10^{4}	//(010)	8.64×10^{5}	1.18×10^{-21}	-20.93	0.
I-11 I-19	abt	776	g NNO	< 10	//(010)	1.01×10^{6}	4.52×10^{-22}	-21.34	0.

(continued on next page)

Table 1 (continued)

NimpDi-14

NimpDi-8

NimpDi-9

NimpDi-10

NimpDi-11

N-6

N-3

San Carlos olivine									
Expt ID	Type ^a	T(C)	f_{02}^{b}	Bars ^c	Slab ^d	Time (s)	D (m ² /s)	logD	±
N-7	abt	800	g	10 ⁴	//(010)	6.05×10^{5}	2.26×10^{-21}	-20.65	0.33
N-3	abt	850	g	10^{4}	//(010)	2.38×10^{5}	5.69×10^{-21}	-20.25	0.22
N-3R	out	800	NNO	~1	//(010)	9.0×10^{4}	9.0×10^{-22}	-21.05	0.30
N-14	abt	850	NNO	< 10	//(010)	4.07×10^{5}	9.14×10^{-21}	-20.04	0.13
N-22	abt	850	NNO	< 10	//(010)	5.02×10^{5}	7.52×10^{-21}	-20.12	0.25
N-18	abt	900	NNO	< 10	//(010)	1.80×10^{4}	1.35×10^{-20}	-19.87	0.17
N-21	abt	950	NNO	< 10	//(010)	4.91×10^{5}	2.70×10^{-20}	-19.68	0.15
Clinopyroxene ^e									
Expt ID	Type ^a	T(C)	f_{02}^{b}	Bars ^c	Slab ^d	Time (s)	D (m ² /s)	logD	±
NimpDi-6	impl	751	NNO	1	//(110)	1.87×10^{6}	5.84×10^{-22}	-21.23	0.10
NimpDi-2	impl	801	NNO	1	//(110)	8.64×10^{5}	3.29×10^{-21}	-20.48	0.10
NimpDi-1	impl	850	NNO	1	//(110)	4.25×10^{5}	4.22×10^{-21}	-20.37	0.10
NimpDi-3	impl	901	NNO	1	//(110)	2.52×10^{5}	8.02×10^{-21}	-20.10	0.10
NimpDi-4	impl	952	NNO	1	//(110)	1.73×10^{5}	9.10×10^{-21}	-20.04	0.22
NimpDi-5	impl	1001	NNO	1	//(110)	8.28×10^{4}	2.87×10^{-20}	-19.54	0.10
NimpDi-7	impl	1050	NNO	1	//(110)	6.84×10^{4}	3.19×10^{-20}	-19.50	0.10
NimpDi-12	impl	1100	NNO	1	//(110)	7.56×10^4	2.96×10^{-20}	-19.53	0.24
NimpDi-13	impl	1100	NNO	1	//(110)	1.53×10^{5}	1.83×10^{-20}	-19.74	0.15
NimpDi-15	impl	1100	NNO	1	//(110)	1.44×10^{4}	3.36×10^{-20}	-19.47	0.14

//(110)

//(110)

//(110)

//(110)

//(110)

//(110)

//(110)

 2.88×10^{4}

 2.88×10^{4}

 1.89×10^4

 9.90×10^{3}

 7.20×10^{3}

 5.74×10^{5}

 2.38×10^{5}

 4.43×10^{-20}

 8.85×10^{-20}

 1.24×10^{-19}

 1.93×10^{-19}

 3.03×10^{-19}

 7.33×10^{-22}

 5.69×10^{-21}

-19.35

-19.05

-18.91

-18.71

-18.52

-21.14

-20.25

0.13

0.12

0.10

0.15

0.10

0.27

0.22

NNO

NNO

NNO

NNO

NNO

1

1

1

 10^{4}

10

impl

impl

impl

impl

impl

abt

abt

1100

1150

1200

1251

1299

800

850

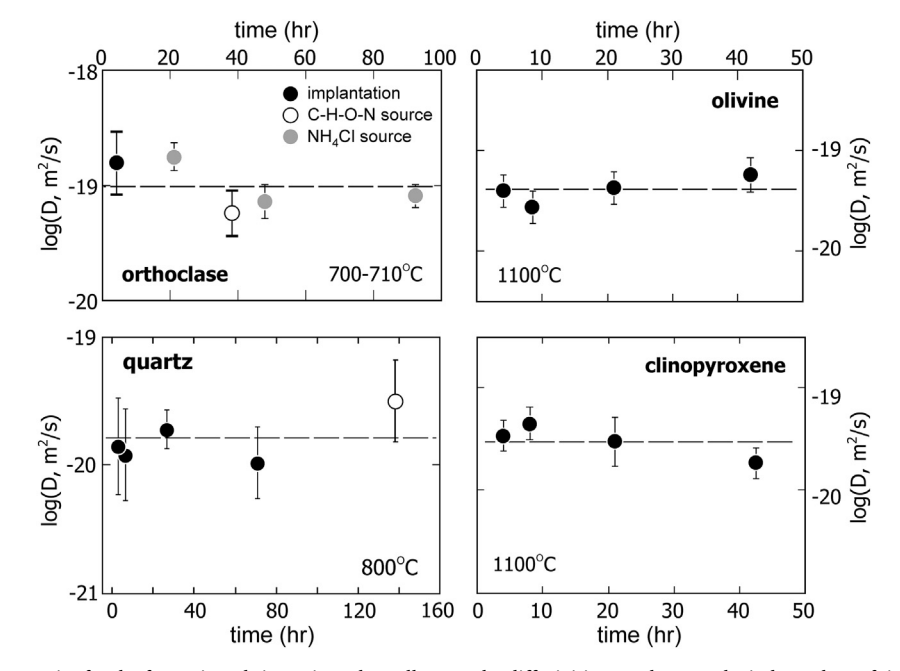


Fig. 7. Results of diffusion time series for the four minerals investigated. In all cases, the diffusivities are shown to be independent of time within error. Uncertainties are \pm 1 standard deviation.

^a Experiment types: abt = aminobutyric acid vapor (or fluid) source; gly = glycine vapor (or fluid) source; impl = implantation experiment; NH₄Cl = molten NH₄Cl source; out = out diffusion experiment performed on a previous in-diffused (abt) sample (N-3 olivine).

^b Oxygen fugacities: NNO = Ni-NiO; IW = iron-wüstite; g = equilibrium with graphite.

^c The pressure is not exactly known for experiments conducted in silica glass ampoules containing C-H-O-N vapor produced by decomposition of amino acids (see text), but is unlikely to exceed 10 bars due to strength limitations of the glass, hence the designation " < 10 bars" for these experiments.

^d Orientation of the polished mineral slab.

^e All de Kalb diopside except experiment N-3, which was Templeton augite.

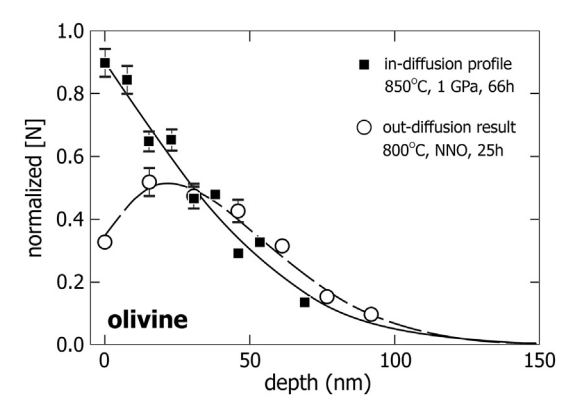


Fig. 8. Nitrogen-15 uptake profile in San Carlos olivine obtained at 850 °C (black squares; experiment no. N-3) compared with the profile obtained by reannealing the same sample at 800 °C for 25 h (open circles; experiment no. N-3R). Note that the re-heating causes loss of in-diffused ¹⁵N from the surface as well as penetration deeper into the sample, as expected. The diffusivities implied by the two profiles are consistent with the overall data set for olivine.

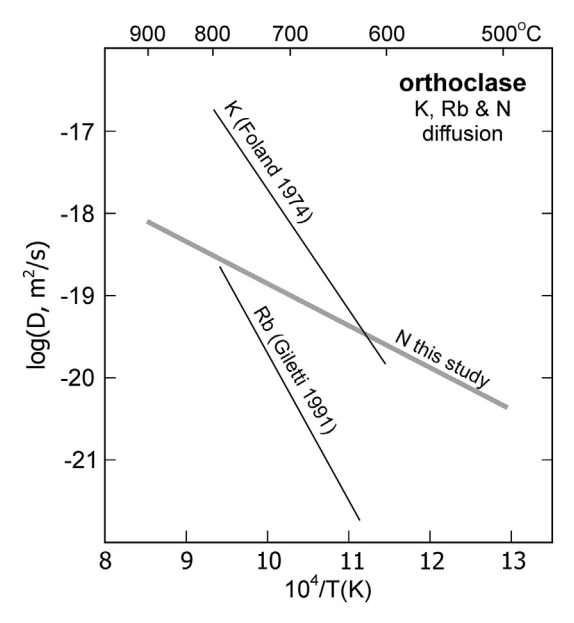


Fig. 9. Comparison of the Arrhenius law for N diffusion in orthoclase obtained in the present study with those for K and Rb obtained by previous researchers (Foland, 1974; Giletti, 1991). The marked difference in slope (activation energy) suggests that N diffusion is more complicated than simple $NH_4^+ \leftrightarrow K^+$ exchange. See text for discussion.

puzzling in some respects, but also welcome because the other three minerals of our study do not contain K and therefore do not have obvious sites to accommodate the large NH₄ ion at low pressures—so an additional mechanism for N incorporation is needed in those cases, too. The exact size of the ammonium ion seems to be open to debate. A recent study by Sidey (2016), for example, places the radius between those of K+ and Rb+, but Watenphul et al. (2009) argue for a substantially larger radius falling between Rb⁺ and Cs⁺ (Fig. 10). Either way, NH₄ is predicted to be largely excluded from clinopyroxene (at low pressure), olivine and quartz, because all three bracketing alkalies (K, Rb, Cs) are highly incompatible in these minerals. Based on the Wood and Blundy (1997) lattice-strain treatment, for example, the clinopyroxene/melt partition coefficient for NH_4^+ is ~ 0.002 using the Sidey (2016) radius of 0.154 nm (for 8-fold coordination) and ~0.0001 using the Watenphul et al. (2009) radius of 0.168 nm. Watenphul et al. (2010) have demonstrated that NH₄⁺ does indeed enter clinopyroxenes at pressures markedly higher than those of the present study

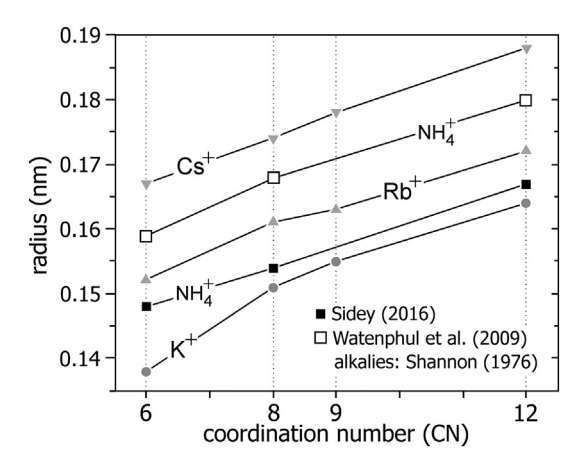


Fig. 10. Two estimates of ionic radii for $\mathrm{NH_4}^+$ (Watenphul et al., 2009; Sidey, 2016) compared with those for K^+ , Rb^+ and Cs^+ (Shannon, 1976). The comparison implies that the ammonium ion is highly incompatible in clinopyroxene (at low pressure) and olivine, because the bracketing alkalies are extremely incompatible.

(9.5–12.8 GPa), but we have no way to conduct and analyze diffusion experiments at such pressures. Judging from the very low concentrations of K, Rb and Cs in natural olivines and quartz crystals, the prospects for diffusive uptake of $\mathrm{NH_4}^+$ in those minerals seem very unlikely.

The elimination of NH₄⁺ as the probable dominant N-carrying diffusant in olivine, clinopyroxene and quartz raises the question as to just what the diffusing entity is, and how N is incorporated into the mineral structures at the low pressures of this study. Unfortunately, we cannot determine the speciation of N dissolved in our run products using FTIR or other spectroscopic techniques because the thickness (depth) of the region containing in-diffused N is limited to ~300 nm. For this reason, arguments regarding speciation must be circumstantial and somewhat speculative. A key observation is that the diffusivities we measure do not depend on how N is introduced into the minerals (i.e., whether by in-diffusion from C-H-O-N vapor or by ion implantation): diffusively mobile N atoms in the mineral structure have no "memory" of how they were introduced. For a given mineral, the similarity in diffusivities from various kinds of experiments-some "wet", some "dry"-also indicates that H is probably not involved in N diffusion, a conclusion that reinforces the NH₄⁺ incompatibility argument in the previous paragraph. The decoupling from H also appears to rule out neutral NH₃ molecules, which is consistent with the suggestion (Section 2.3) that the f_{O2} -buffered conditions of the C-H-O-N-source experiments are too oxidizing for ammonic forms of N to be stable (Mikhail et al., 2017). We are thus led to the tentative conclusion that N is present in the mineral structures as N₂ molecules. This is consistent with the very strong N≡N bond, and the modest activation energies for diffusion (~100–140 kJ/ mol) suggest that these bonds are not broken during diffusive jumps (ΔH for breaking the N≡N bond is nearly 1000 kJ/mol; Cotton and Wilkinson, 1972). Because implanted N shows the same diffusion behavior as in-diffused N, we tentatively conclude that implanted N atoms form N2 as soon as they are mobilized in the structure by heating the sample. That said, we cannot rule out the possibility that monatomic N is the diffusing species. This suggestion might seem unlikely (or irrelevant) given that possible nitrogen species in deep-seated C-H-O-N fluids are limited to N2, NH3 and NH4+ (Mikhail et al., 2017). The model calculations of these authors indicate that the speciation of N in subduction-zone fluids is dominated by either N2 or NH4+, depending on the specific conditions of P, T, $f_{\rm O2}$ and pH (N₂ is favored in shalllower, hotter subduction environments). It is important to bear in mind, however, that the speciation of N dissolved in minerals need not correspond to the dominant N species in a coexisting fluid. A simple example is that of "water" in nominally anhydrous minerals (NAMs), in

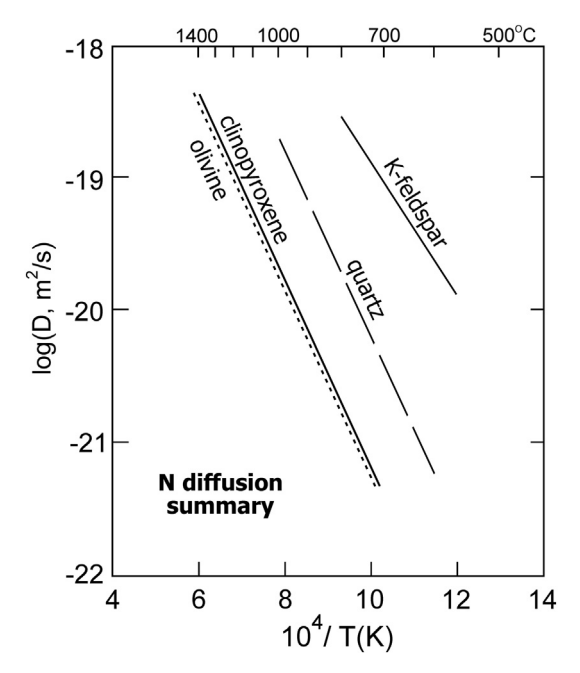


Fig. 11. Summary and comparison of diffusion laws for N in the four minerals included in the present study. The marked differences become significant in considering the relative N retentivities of these minerals in the crust and mantle.

which the dissolved species is mostly OH⁻ when the external fluid is H₂O (e.g., Johnson, 2006; Beran and Libowitzky, 2006).

3.3. Comparative N diffusion among minerals and to other diffusants

Fig. 11 is a summary of the Arrhenius lines for N diffusion in the

500°C 400°C -15 -17 a b quartz orthoclase -18 -16 (O vs. N) (O & Ar vs. N) -19 $og(D, m^2/s)$ -18 -21 -19 -20 -23 -21 -24 -25^L -22 10 11 12 13 16 14 6 8 10 12 14 10⁴/T(K) 10⁴/T(K) 700°C -16 1300 1000 800 700°C 1400 900 -16 c d clinopyroxene olivine (O & Ar vs. N) (O & Ar vs. N) -17 -17 Ar (Cassata et al. 2011) -18 $^{-18}_{-18}$ (S/ $^{-18}_{-18}$ $log(D, m^2/s)$ -20 -20 -21 Ar (Thomas et al. 2008) -21 -22 10 10 104/T(K) 10⁴/T(K)

four minerals investigated in this study. Nitrogen diffuses slowest in olivine and clinopyroxene and at nearly the same rate in these two minerals, with an activation energy $E_{\rm a}$ of \sim 135–140 kJ/mol (see Eq. (3) and Fig. 6). The activation energy for N diffusion in quartz is similar (147 kJ/mol), but the substantially higher pre-exponential factor ($D_{\rm 0}$ in Eq. (3)) means that N diffuses more than an order of magnitude faster in the more open-structured quartz than in the mafic minerals. Nitrogen diffusion in orthoclase is still faster, and the lower activation energy means that the difference in D between orthoclase and the other minerals increases with falling temperature. This effect will prove to be important in models of N diffusion in natural systems (Section 4).

If, as our data suggest, N does not diffuse as NH₄⁺ mimicking large alkali ions (Section 3.2 and Fig. 9), the question arises as to whether there exist similarities to any non-cationic diffusants—possibly oxygen or noble gases. Nitrogen and oxygen are both strongly electronegative elements that form extremely stable diatomic molecules. In the presence of H₂O, oxygen is generally believed to diffuse rapidly in openstructured silicates as mobile (neutral) H₂O molecules that hydrolyze Si-O bonds to produce OH within the mineral structure (e.g., Farver and Yund, 1991; Zhang et al., 1991). Under dry conditions oxygen diffusion may involve migration of O²⁻ ions, probably via an oxygen vacancy mechanism (Farver, 2010). In quartz and orthoclase, the Arrhenius law for N diffusion is intermediate between the widely separated sets of "wet" and "dry" Arrhenius lines for oxygen (Fig. 12a&b). Despite significant scatter in the existing oxygen data for these minerals, the activation energy for N diffusion is generally comparable to that for "wet" oxygen diffusion, but N is ~1-2 orders of magnitude slower on average. Nitrogen diffusion in clinopyroxene and olivine is broadly similar to "dry" oxygen diffusion in these minerals at 1000°-1400°C (Fig. 12c&d); however, the activation energy for N diffusion is substantially smaller, which means that N is more mobile than O at lower temperatures.

Comparison of the new N diffusion measurements with data for noble gases is difficult because of the scatter in the noble gas data (see

Fig. 12. Comparison of the Arrhenius laws for N diffusion from the present study with oxygen and argon laws published by previous workers. The published data are from the summaries of Farver (2010) for oxygen and Baxter (2010) for noble gases. The Ar in clinopyroxene line in panel c is from Cassata et al. (2011). The shaded regions in panels a and b separate "wet" and "dry" Arrhenius laws for oxygen. See text for discussion.

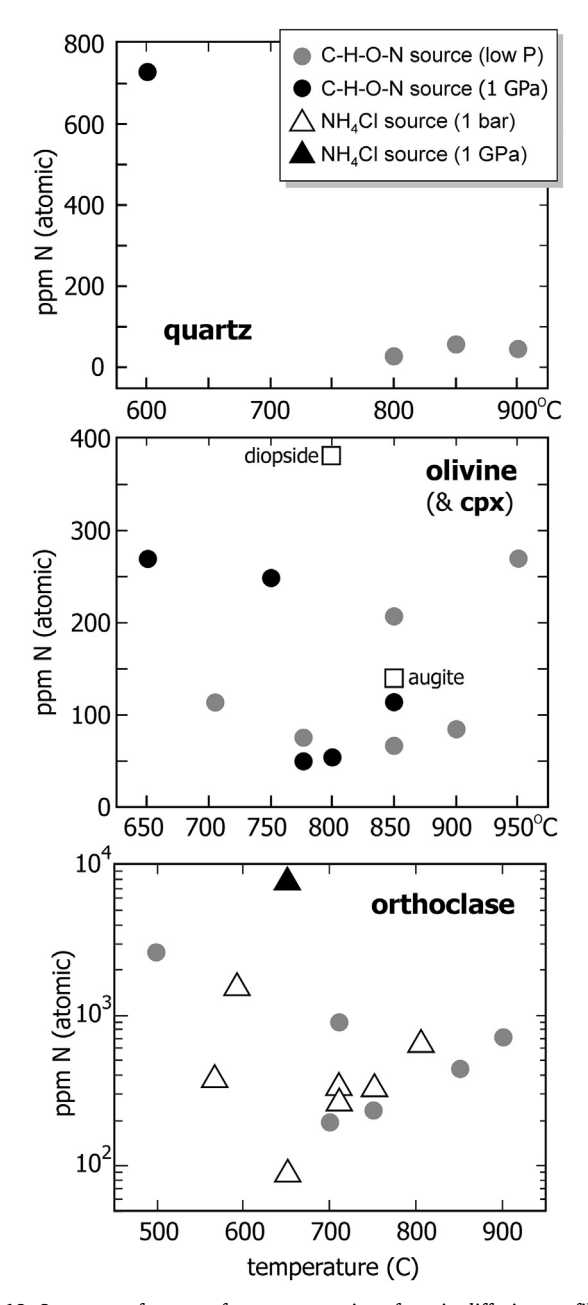


Fig. 13. Summary of near-surface concentrations from in-diffusion profiles of ¹⁵N in quartz, olivine, clinopyroxene and orthoclase (see Fig. 5). Results for orthoclase were obtained from samples immersed in C-H-O-15N vapor and (separately) in molten ¹⁵NH₄Cl; results for the other minerals are from experiments using the C-H-O-15N source only. Note that only two results were obtained for clinopyroxene so these are plotted on the olivine panel (open squares). In general, the concentrations indicate modest but significant compatibility of N in all minerals. It is important to note, however, the we consider the values to be only qualitative indicators of N partitioning or solubility behavior. The pressure of the C-H-O-N vapor (hence the partial pressure of N2) is not exactly known, and some open-system behavior is expected in the vaporsource experiments, given the permeability of silica glass to H₂O and especially H₂. There is, in addition, substantial uncertainty in the estimated near-surface concentrations obtained by NRA. Inaccuracies arising from these effects may explain the lack of perceptible correlations between [N] and pressure or temperature. See text for discussion.

Baxter, 2010)—which may be due in part to the disparate methods that have been used to characterize noble gas diffusion (mainly bulk degassing, but including some direct profiling measurements by laser ablation, Rutherford backscattering and NRA). The most logical

comparison for N is specifically with Ar because of the similarity in size of N₂ and Ar molecules (Hirschfelder et al., 1954). Selected Arrhenius lines for Ar diffusion in orthoclase and olivine are included in Fig. 12b&d for comparison with N. In olivine, N diffusion falls in between the Ar measurements of Futagami et al. (1993) and Thomas et al. (2008), with E_a similar to that of Futagami et al. (1993) for Ar. Nitrogen is slower than Ar in orthoclase—by ~3 orders of magnitude at 800 °C and 1–1.5 orders of magnitude at 500 °C. These generalizations do not necessarily hold for other choices of Ar Arrhenius lines from the literature, which vary substantially (for orthoclase we used the representative K-feldspar average of Baxter, 2010; see Fig. 12b).

3.4. Qualitative N partitioning

As noted previously, experiments involving N diffusion into minerals from external media (C-H-O-N vapor or NH₄Cl) have the potential to provide insight into the partitioning of N between crystals and their N-rich surroundings, provided the near-surface concentrations and the nature of the N-bearing medium can be accurately characterized. In the present diffusion-focused study, surface-uptake concentrations of N must be regarded as only qualitative indicators of equilibrium (see Sections 2.3 and 2.9), but we report the results here to show broad consistency with experimental and analytical studies of N in minerals. Fig. 13 summarizes estimated near-surface concentrations of N (C_o values in Eq. (1)) for 32 in-diffusion experiments. There are few if any systematic dependencies in the data, so N concentrations (in ppm atomic) are plotted against temperature for lack of a more compelling choice. In the case of quartz, the C_o values of 30–60 ppm obtained from relatively high-T, low-P experiments (800-900 °C; < 10 bars) are much smaller than the one value obtained at relatively low T and high P (600 °C; 1 GPa), where the concentration is ~700 ppm. This difference might be logically attributable to the difference in P_{N2} between the lowand high-temperature experiments, but it is also conceivable that a difference in pH may have played a role, given that quartz is more soluble in high-pressure C-H-O-N fluid and quartz dissolution would be expected to lower the pH [Mikhail et al., 2017 showed that pH can influence N speciation in a C-H-O-N fluid]. Unfortunately—because the amino-acid derived C-H-O-N vapor contains H2O-simultaneous high-P, high-T are not possible with quartz due to the substantial solubility of this mineral in hydrous fluid at elevated P. It is clear, nevertheless, that quartz is capable of incorporating N from hydrous, N-rich fluid at levels exceeding 100 ppm. In the case of olivine, near-surface N concentrations range from ~50 to ~270 ppm ($\bar{x} \cong 140$ ppm, $\sigma \cong 90$ ppm) for the full range of P-T conditions investigated, with no systematic dependence on P or T (Fig. 13). For the two in-diffusion experiments performed on clinopyroxene (one on diopside; one on augite), the C_o values are 380 and 140 ppm, respectively. The values generally exceed those in mafic minerals from high-pressure experiments on N₂ solubility (e.g., Li et al., 2013) and measurements on natural samples (e.g., Busigny et al., 2011)—with the important exceptions of sheet silicates and "open-channel" microporous silicates such as beryl and cordierite (Bebout et al., 2016).

Of the minerals investigated in this study, orthoclase stands out as by far the most accepting of N, with near-surface concentrations ranging from ~ 100 ppm to nearly 0.8% (note the log scale for N in orthoclase in Fig. 13). This result was anticipated because of the known exchangeability of NH₄ $^+$ and K $^+$ in feldspar and the high N concentrations observed in some natural samples—although ultimately our depth-profiling results revealed that the chemical diffusion phenomenon is not a simple exchange of NH₄ $^+$ for K $^+$ (see Section 3.2) under the conditions of our experiments. For major rock-forming silicates in general, a key (if only qualitative) conclusion from our diffusion study is that N compatibility is limited but significant at crustal and upper mantle conditions. This finding confirms earlier lines of evidence that the lithosphere is a major global reservoir of nitrogen (e.g., Busigny et al., 2003; Li et al., 2013; Johnson and Goldblatt, 2015; Bebout et al.,

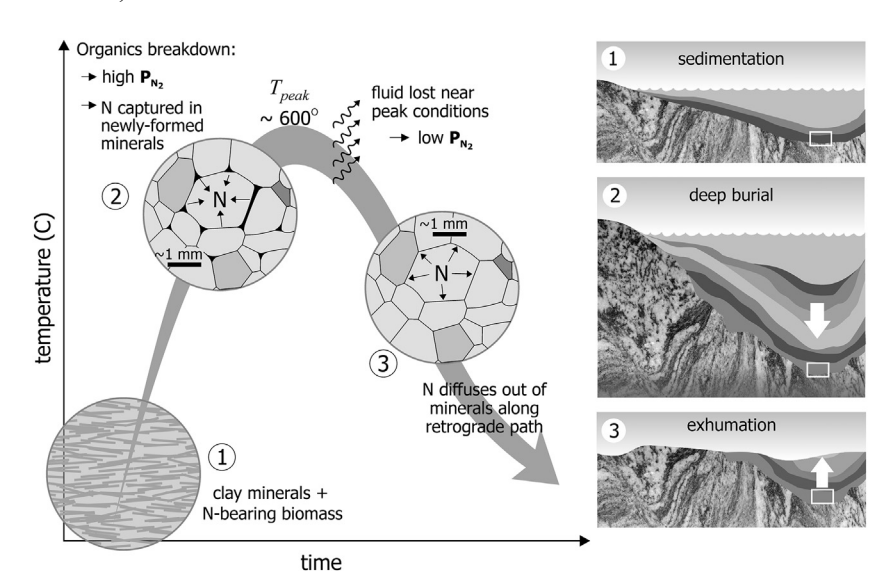


Fig. 14. Schematic of a time-temperature (*t-T*) path that involves the following sequence: (1) burial of sediment containing N-bearing biomass; (2) prograde heating (with implied increase in pressure) to promote N uptake in minerals from biomass-generated fluid, then loss of fluid near peak conditions; and (3) out-diffusion of N from minerals on the retrograde limb. The numbered panels at the right are cartoon depictions of these steps. See text.

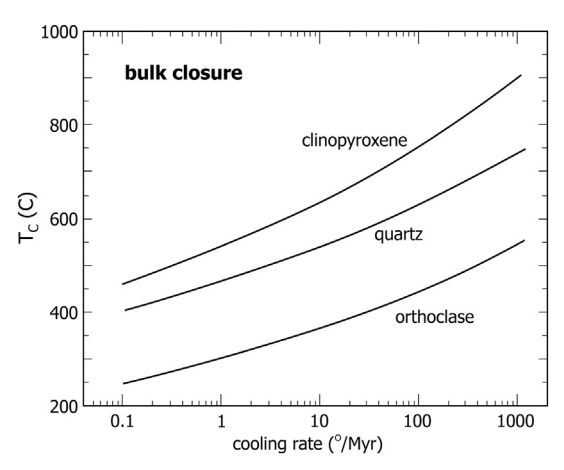


Fig. 15. Bulk closure temperature for nitrogen (T_{C_i} : Dodson, 1973) as a function of cooling rate for minerals of 1 mm radius. See text for implications.

2016; Houlton et al., 2018).

4. Implications for N transport and cycling in the lithosphere

4.1. Metamorphic "processing" of biogenic N in the continental crust

The primary motivation for characterizing diffusion laws is to enable modeling of transport in geologic systems that cannot be studied directly due to inaccessibility in space or time. Given the recent interest in bioavailable N from the continental crust (e.g., Houlton et al., 2018) and recycling of N into the mantle (Johnson and Goldblatt, 2015), we explore two N transport scenarios using simple numerical models to address: 1) the diffusive release of N from continental crustal minerals undergoing exhumation; and 2) the dispersal of subducted N in the upper mantle.

Fig. 14 is a cartoon depicting a simple temperature-time path followed by a parcel of sediment that is buried and heated to $600\,^{\circ}$ C, then exhumed and returned to near-surface conditions. The sediment initially contains N-bearing biomass (location no. 1 on the t-T path), some fraction of which is retained as interstitial N₂-bearing fluid to relatively high-grade metamorphic conditions. As the assumed peak temperature of $600\,^{\circ}$ C is approached, N is moderately partitioned into the silicate minerals of the evolving metamorphic assemblage (location 2). At a peak temperature (T_{peak}) of $600\,^{\circ}$ C, the N₂-bearing fluid leaves the system, so when exhumation induces cooling along the retrograde limb

of the t-T path, there is minimal partial pressure of N_2 (P_{N2}) to "support" the mineral-hosted N_2 , which escapes from the minerals to whatever extent is allowed by diffusion (location 2). One way to assess N_2 loss from minerals cooling from high temperature is to insert our new Arrhenius parameters for N diffusion (D_0 and E_a) into the Dodson (1973) equation describing the bulk closure temperature, T_C , as a function of grain radius (a) and cooling rate (dT/dt):

$$T_C = \frac{E_a/R}{ln \left[\frac{55RT_C^2 D_0/a^2}{E_a \cdot dT/dt} \right]}.$$
(4)

(the constant 55 is a geometric factor for diffusion in a sphere). In Fig. 15, closure temperatures for clinopyroxene, quartz and orthoclase crystals of 1 mm radius are plotted for cooling rates ranging from 1 to 1000°/Myr. For a tectonically realistic cooling rate of 30°/Myr, the closure temperatures for orthoclase, quartz and clinopyroxene are 400°, 580° and 685°C, respectively—suggesting that clinopyroxene should retain N quite well during cooling from 600°C, but orthoclase would experience major N loss.

The magnitudes of N losses from cooling minerals are better appreciated with reference to Fig. 16, which shows the results of finitedifference calculations of diffusive loss during cooling from 600 °C for two exponential cooling scenarios given by the equation shown in the upper left panel of the figure (in this cooling model, the initial temperature T_i is the same as T_{peak} on the t-T path shown in Fig. 14). The other panels in Fig. 16 are graphs of fractional loss, F, of nitrogen from clinopyroxene, quartz and orthoclase (1 mm radius) cooled from 600 °C at initial rates of 10° and 100 °C/Myr. At the slower cooling rate, Kfeldspar loses essentially all of its initial N within the first $\sim 5^{\circ}$ of cooling, whereas clinopyroxene loses only ~30% over the entire cooling interval. Quartz falls in between K-feldspar and clinopyroxene in terms of N retentivity. The faster cooling rate (100 °C/Myr) results in significantly better retention for all three minerals, but even in that case, orthoclase loses ~98% of its initial N within the first 100° of cooling. Importantly, if T_i were higher than the assumed 600 °C, diffusive N losses would be greater than those shown in Fig. 16; lower T_i would result in smaller losses and allow K-feldspar to retain some N through the exhumation cycle.

The model and calculations illustrated in Figs. 14–16 suggest a possible cycling or "processing" of nitrogen in the continental crust that is linked to metamorphic cycles as shown in Fig. 17. Deep burial of biomass-laden sediments leads to N incorporation into metamorphic silicate minerals ("inhalation" of N; top panel); post-peak, fluid-absent exhumation triggers some diffusive loss from minerals on the retrograde limb of the *t-T* path ("exhalation" of N; bottom panel), the extent

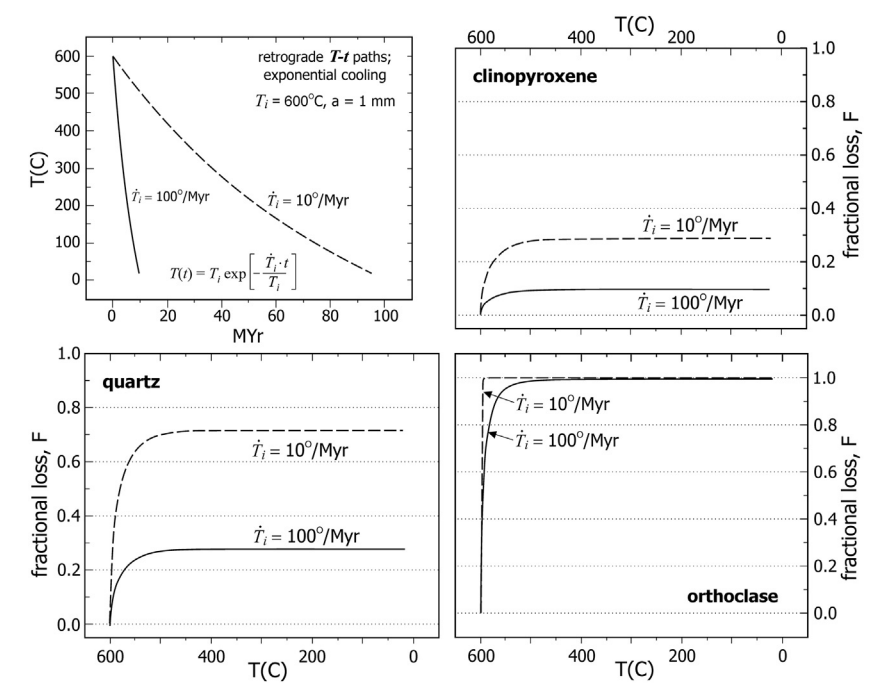
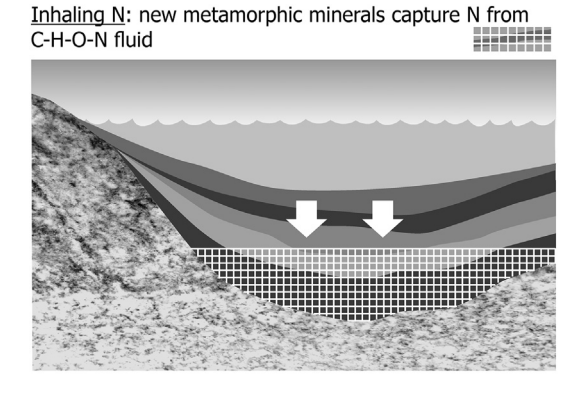


Fig. 16. Illustrations of diffusive closure behavior for orthoclase, quartz and clinopyroxene during cooling from 600 °C. The upper left panels shows the two exponential cooling paths considered, one with an initial cooling rate $(\dot{t_i})$ of 100° /Myr (solid curve), the other with $\dot{t_i} = 10^\circ$ /Myr (dashed curve). The other three panels show the fractional loss (F) of N from mineral grains of 1 mm radius as a function of temperature for the two cooling paths. See text for discussion.



Exhaling N: N released from minerals during exhumation

diffusion out of minerals

mineral weathering

Fig. 17. Cartoon suggesting a possible mechanism for cycling of N in the continental crust through uptake of biogenic N in metamorphic minerals during burial and heating, followed by eventual release to the biosphere via diffusion (and ultimately weathering) on the retrograde limb of the *t-T* path. The latter processes might provide the N flux into the biosphere called upon by Houlton et al. (2018) to compensate marine N burial.

of which depends on T_{peak} , cooling rate, and the specific minerals involved. Continued exhumation transports diffusively retained N back to the surface, where it is liberated by mineral weathering. The latter two phenomena-diffusive loss during exhumation and mineral weathering—could constitute the specific delivery mechanisms for the 14-34 teragram/year flux of bioavailable N from the crust (the "rock nitrogen source") hypothesized by Houlton et al. (2018) to balance marine burial of N in the terrestrial N cycle. Interestingly, the two mechanisms of releasing N from minerals have markedly different implications for N isotopes: N release by mineral weathering should have no effect on N isotopes, but partial outgassing of minerals by diffusion would probably favor ¹⁴N over ¹⁵N, leaving an elevated ¹⁵N/¹⁴N remaining in the mineral. [Note: To our knowledge, there exists no direct evidence that 14N diffuses faster than 15N in minerals, but an isotope mass effect on diffusion has been confirmed for numerous elements in a variety of condensed materials, including Cl, Mg, Ca, Fe Li in silicate melts (Fortin et al., 2017; Watkins et al., 2009, 2011; Richter et al., 2003; Holycross et al., 2018), Li in pyroxene and olivine (Richter et al., 2014; Richter et al., 2017), Mg and Fe in olivine (Sio et al., 2018), He in diamond (Cherniak et al., 2018a, 2018b), Fe and Ni in iron meteorite alloys (E.B. Watson et al., 2016; H.C. Watson et al., 2016), C in Fe (Müller et al., 2014), Li, Mg Na, K, Cs and Ca ions in water (Bourg et al., 2010), and numerous elements in metal alloys (see summary in Richter et al., 2009)]. An isotope mass effect on N diffusion could explain the observation of Haendel et al. (1986) that N concentration in contact metamorphic rocks decreases toward a granitic pluton-perhaps implying diffusive loss from the assemblage with increasing temperature—while $\delta^{15}N$ increases (implying that ^{14}N is preferentially lost due to faster diffusion).

A final diffusion calculation concerning N in the continental crust addresses the question of N storage in tectonically inactive regions over geologic time. From analyses of glacial tills, Johnson and Goldblatt (2017) concluded that N is sequestered in the continental crust for geologically long time periods, and that [N] has increased progressively from the Archean to the current (Phanerozoic) value of 380 \pm 50 ppm. Assuming bulk N retention in the crust is controlled by volume diffusion within mineral grains, our diffusion data can be used to address long-

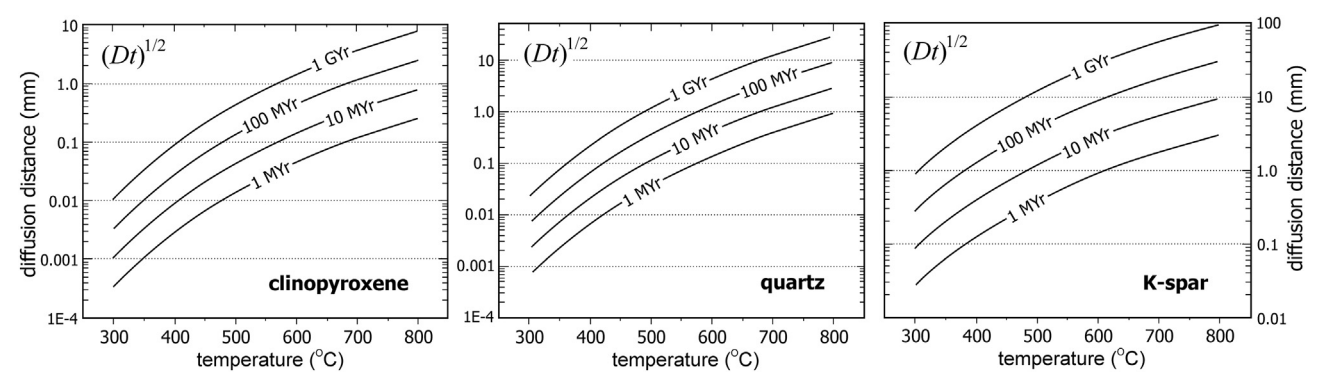


Fig. 18. Characteristic diffusion distances ($=Dt^{1/2}$) for N in clinopyroxene, quartz, and K-feldspar for a range of crustal temperatures and durations ranging from 1 MYr to 1 GYr. Diffusion distances smaller than the typical grain size of crustal rocks imply effective N sequestration in the continental crust. See text for discussion.

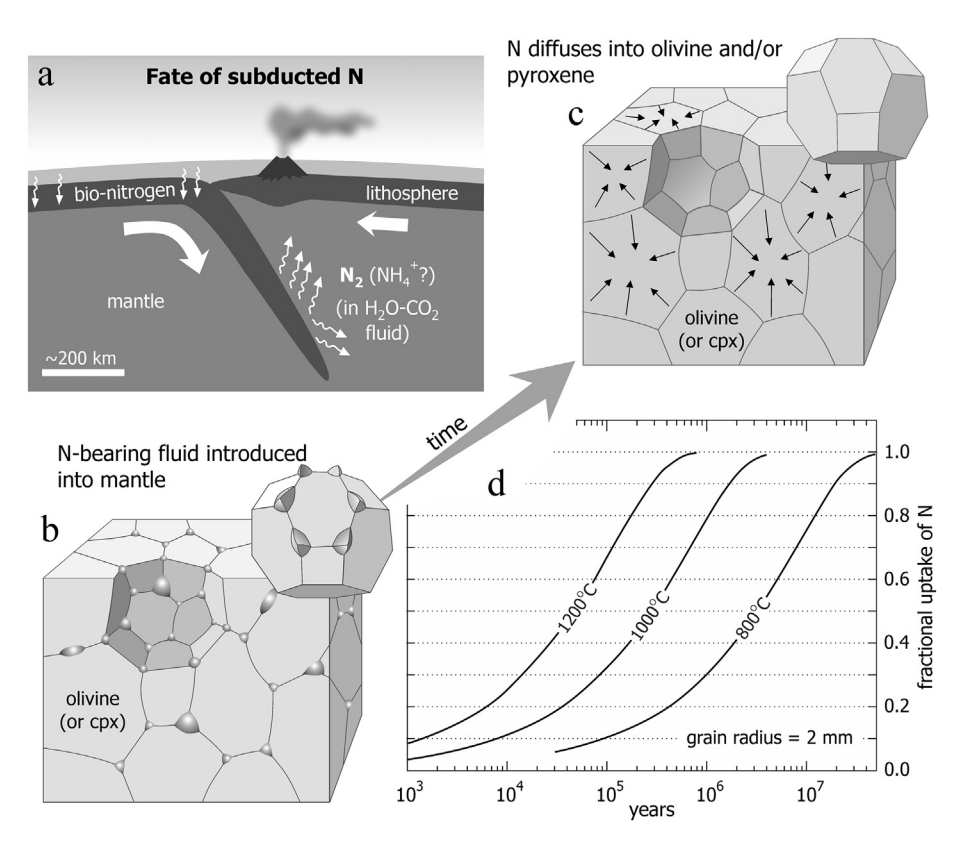


Fig. 19. Hypothetical dispersal and sequestering of subducted N in mantle minerals via diffusion. The tectonic setting is depicted in a, the grain-scale processes are illustrated in b and c, and the rate of diffusive N uptake for grains of 2 mm radius at 800°, 1000° and $1200\,^\circ$ C is shown graphically in d. The curves in d apply to both olivine and clinopyroxene because the diffusion laws for the two minerals are nearly the same. The curves could equally well apply to fractional *loss* if there were a local sink for N. See text for additional discussion.

term storage by computing Dt/a^2 for any assumed temperature and relating the result to the fractional loss, F (see, e.g., Fig. 6.1 of Crank, 1975). For example, $Dt/a^2 = 0.03$ corresponds to 50% N loss. A simpler parameter bearing on long-term retention is the characteristic diffusion distance $(Dt)^{\frac{1}{2}}$: if the value of this parameter is smaller than the estimated grain size of N-bearing minerals in the continental crust, then substantial N retention is indicated. As discussed previously, clinopyroxene is the most retentive of the four minerals for which we have data. For clinopyroxene, $(Dt)^{1/2}$ at 500 °C for t = 1 GYr is ~ 0.4 mm—implying significant long-term retention, consistent with the conclusions of Johnson and Goldblatt (2017). At the fast-diffusion extreme, the characteristic diffusion distance (Dt)1/2 of N in K-feldspar for the same thermal history is ~12 mm, which exceeds typical grain sizes and indicates ineffective retention. Characteristic diffusion distances for a wide range of other t-T scenarios are shown in Fig. 18. The broad conclusion is that diffusion distances significantly smaller than the typical grain sizes of crustal rocks are indicated for a wide range of midcrustal temperatures (300-500 °C) over vast geologic time. Long-term sequestration of N in the continental crust is therefore entirely

plausible.

We note in closing this discussion of "metamorphic" N cycling that our simple metamorphism/diffusion scenario may be unrealistic for situations involving muscovite-dominated pelitic assemblages. Micas are known to incorporate significant amounts of N (e.g., Higashi, 1978; Duit et al., 1986; Boss et al., 1988; Ruiz Cruz and Sanz de Galdeano, 2008), so the stability of muscovite on the retrograde limb of the t-T path could mean that the behavior of N in the rock is regulated largely by this mineral. In this case, knowledge of the diffusion law for N in muscovite becomes important to models of N cycling. Unfortunately, our direct profiling technique is not suitable for the characterization of N diffusion in micas because of the dominant and unavoidable (001) cleavage. We might be successful measuring N diffusion \bot (001), but the phenomenon of real interest would be layer-parallel diffusion, which is almost certainly much faster [see, e.g., the study of Fortier and Giletti, 1991 on oxygen diffusion in micas].

4.2. Fate of subducted N in the mantle

Our measurements of N diffusion in olivine and clinopyroxene can be used to place constraints on the diffusive mobility of N in the upper mantle. A plausible scenario to consider is a subduction setting in which N-bearing fluid is introduced into the mantle wedge through breakdown of minerals containing H2O, CO2 and N (Fig. 19a; see, e.g., Sadofsky and Bebout, 2004; Busigny et al., 2011; Bebout and Penniston-Dorland, 2016). Our modeling cannot address isotopic effects at this time, so the ultimate source of N could be either sediment-hosted biomass or altered oceanic crust (see, e.g., Halama et al., 2014). Depending on whether the released C-H-O-N fluid is wetting or non-wetting with respect to olivine and/or clinopyroxene grain edges, it would form either interconnected or isolated porosity in the host rock (Watson and Brenan, 1987; Watson et al., 1990; Mibe et al., 1999). The former could promote relatively long-range N transport by porous flow; the latter would result in fluid stagnation and only local dispersal of N and other fluid-borne elements mainly by diffusion. The wetting properties of Nbearing fluids have not been characterized, but aqueous fluids containing more than 10 or 20% CO₂ are likely to be non-wetting at the P-T conditions under consideration here (Watson and Brenan, 1987; see lower left panel of Fig. 19b). In either case, the introduction and stable storage of N in the lattices of mantle minerals would require volume diffusion as governed by our measured Arrhenius laws.

Fig. 19d shows the results of diffusive-uptake calculations for N in spherical olivine grains of 2 mm radius (calculations for clinopyroxene yield very similar results). Three isothermal cases are considered (800°, 1000° and 1200°C), and the results are plotted as fractional uptake of N as a function of time. At 800 °C, the time required for the fractional uptake to reach 0.5 (i.e., 50% "nitrogenation" of olivine) is ~3 Myr, and full uptake (N saturation) requires ~60 Myr. These times are shortened by roughly an order of magnitude for each 200 °C increase in temperature, such that at 1200 °C, 50% N uptake is achieved in ~0.04 Myr and N saturation in ~0.8 Myr. These time scales seem sufficiently short to conclude that mantle minerals take in a significant amount of N from contacting fluid released in subduction settings. The fate of this olivineor pyroxene-hosted N depends on the subsequent t-T history of the host minerals in the mantle and whether they participate in partial melting. Given a low-P_{N2} situation arising from partial melting (for example), N might be lost from mantle minerals by volume diffusion. Fig. 19d would still apply in this case, with the y axis relabeled "fractional loss of N" rather than "fractional uptake".

The broad conclusion from Fig. 19d is that grain-scale equilibration of mantle phases with respect to N is geologically quite fast. The figure also implies, however, that transport of N in the mantle on the outcrop or regional scale by diffusion alone is unrealistic, and would require some combination of fluid flow and diffusion.

Acknowledgements

This work was supported by the U.S. Department of Energy, Office of Science, Office of Basic Energy Sciences, Chemical Sciences, Geosciences and Biosciences Division under Award no. DE-SC0016449 to EBW, and by the Deep Carbon Observatory. Max Drexler was supported by an RPI Summer Undergraduate Research Participation fellowship. We thank Christopher Hoff for the gaseous molecular species calculations discussed in Section 2.3, Wayne Skala and Hassaram Bakrhu for assistance with the ion implantation, and Sarah Dillon for assistance with the SIMS analyses. The latter were made possible in part by National Science Foundation support of the ASU SIMS facility through grant no. EAR 1352996.

References

Baxter, E.F., 2010. Diffusion of noble gases in minerals. In: Zhang, Y., Cherniak, D.J. (Eds.), "Diffusion in Minerals and Melts" Reviews in Mineralogy and Geochemistry.

- vol. 72. pp. 509-577.
- Bebout, G.E., Fogel, M.L., 1992. Nitrogen isotope compositions of metasedimentary rocks in the Catalina Schist, California: implications for metamorphic devolatilization history. Geochim. Cosmochim. Acta 56, 2839–2849.
- Bebout, G.E., Penniston-Dorland, S.C., 2016. Fluid and mass transfer at subduction interfaces—the field metamorphic record. Lithos 240-243, 228–258.
- Bebout, G.E., Cooper, D.C., Bradley, A.D., Sadofsky, S.J., 1999. Nitrogen-isotope record of fluid-rock interactions in the Skiddaw aureole and granite, English Lake District. Am. Mineral. 84, 1495–1505.
- Bebout, G.E., Fogel, M.L., Cartigny, P., 2013. Nitrogen: highly volatile yet surprisingly compatible. Elements 9, 333–338.
- Bebout, G.E., Lazzeri, K.E., Geiger, C.A., 2016. Pathways for nitrogen cycling in Earth's crust and upper mantle: a review and new results for microporous beryl and cordierite. Am. Mineral. 101, 7–24.
- Bell, D.R., Rossman, G.R., Maldener, J., Endisch, D., Rauch, F., 2004. Hydroxide in kyanite; a quantitative determination of the absolute amount and calibration of the IR spectrum. Am. Mineral. 89, 998–1003.
- Beran, A., Libowitzky, E., 2006. Water in natural mantle minerals II: olivine, garnet and accessory minerals. In: Keppler, H., Smyth, J.R. (Eds.), "Water in Nominally Anhydrous Minerals", Reviews in Mineralogy and Geochemistry. vol. 62. pp. 169–191.
- Boss, A., Duit, W., van der Eerden, A.J., Jansen, J.B., 1988. Nitrogen storage in biotite: An experimental study of the ammonium and potassium partitioning between 1M phlogopite and vapor at 2 kb. Geochim. Cosmochim. Acta 52, 1275–1283.
- Bourg, I.C., Richter, F.M., Christensen, J.N., Sposito, G., 2010. Isotopic mass dependence of metal cation diffusion coefficients in liquid water. Geochim. Cosmochim. Acta 74, 2249–2256.
- Boyd, S.R., 2001. Nitrogen in future biosphere studies. Chem. Geol. 176, 1-30.
- Brandes, J.A., Hazen, R.M., Yoder Jr., H.S., 2008. Inorganic nitrogen reduction and stability under simulated hydrothermal conditions. Astrobiology 8, 1113–1126.
- Busigny, V., Bebout, G.E., 2013. Nitrogen in the silicate Earth: speciation and isotopic behavior during mineral-fluid interactions. Elements 9, 353–358.
- Busigny, V., Cartigny, P., Philippot, P., Ader, M., Javoy, M., 2003. Massive recycling of nitrogen and other fluid-mobile elements (K, Rb, Cs, H) in a cold slab environment: evidence from HP to UHP oceanic metasediments of the Schistes Lustrés nappe (western Alps. Europe). Earth Planet. Sci. Lett. 215, 27–42.
- Busigny, V., Cartigny, P., Philippot, P., 2011. Nitrogen isotopes in ophiolitic metagabbros: a re-evaluation of modern nitrogen fluxes in subduction zones and implication for the early Earth atmosphere. Geochim. Cosmochim. Acta 75, 7502–7521.
- Cartigny, P., Marty, B., 2013. Nitrogen isotopes and mantle geodynamics: the emergence of life and the atmosphere-crust-mantle connection. Elements 9, 359–366.
- Cassata, W.S., Renne, P.R., Shuster, D.L., 2011. Argon diffusion in pyroxenes: implications for thermochronometry and mantle degassing. Earth Planet. Sci. Lett. 304, 407–416.
- Cherniak, D.J., Hervig, R., Koepke, J., Zhang, Y., Zhao, D., 2010. Analytical methods in diffusion studies. In: Zhang, Y., Cherniak, D.J. (Eds.), "Diffusion in Minerals and Melts" Reviews in Mineralogy and Geochemistry. vol. 72. pp. 107–169.
- Cherniak, D.J., Thomas, J.B., Watson, E.B., 2014. Neon diffusion in olivine and quartz. Chem. Geol. 371, 68–82.
- Cherniak, D.J., Schaller, M.F., Watson, E.B., 2018a. Nitrogen Diffusion in Calcite. American Geophysical Union Monograph on Deep Carbon. (in press).
- Cherniak, D.J., Watson, E.B., Meunier, V., Karche, N., 2018b. Diffusion of helium, hydrogen and deuterium in diamond: experiment, theory and geochemical applications. Geochim. Cosmochim. Acta 232, 206–224.
- Cotton, F.A., Wilkinson, G., 1972. Advanced Inorganic Chemistry. Interscience Publishers (John Wiley and Sons), New York (1145 pp.).
- Crank, J., 1975. The Mathematics of Diffusion, 2nd ed. Oxford University Press, Oxford (414 pp.).
- Dodson, M.H., 1973. Closure temperature in cooling geochronological and petrological systems. Contrib. Mineral. Petrol. 40, 259–274.
- Duit, W., Jansen, J.B.H., Van Breemen, A., Bos, A., 1986. Ammonium micas in metamorphic rocks as exemplified by Dome de l'Agout (France). Am. J. Sci. 286, 702–732.
- Ewing, R.C., Weber, W.J., Clinard, F.W., 1995. Radiation effects in nuclear waste forms for high-level radioactive waste. Prog. Nucl. Energy 29, 63–127.
- Farver, J.R., 2010. Oxygen and hydrogen diffusion in minerals. In: Zhang, Y., Cherniak, D.J. (Eds.), "Diffusion in Minerals and Melts" Reviews in Mineralogy and Geochemistry. vol. 72. pp. 447–507.
- Farver, J.R., Yund, R.A., 1991. Oxygen diffusion in quartz: dependence on temperature and water fugacity. Chem. Geol. 90, 55–70.
- Foland, K.A., 1974. Alkali diffusion in orthoclase. In: Hofmann, A.W., Giletti, B.J., Yoder, H.S., Yund, R.A. (Eds.), Geochemical Transport and Kinetics. Carnegie Institution of Washington Publication 634. Carnegie Institution of Washington, Washington, D.C., pp. 77–98.
- Fortier, S.M., Giletti, B.J., 1991. Volume self-diffusion of oxygen in biotite, muscovite and phlogopite micas. Geochim. Cosmochim. Acta 55, 1319–1330.
- Fortin, M.-A., Watson, E.B., Stern, R., 2017. Diffusive fractionation of chlorine isotopes in silicate melt and its implications for bubble growth. Earth Planet. Sci. Lett. 480, 15–24.
- Futagami, T., Ozima, M., Nagai, S., Aoki, Y., 1993. Experiments on thermal release of implanted noble gases from minerals and their implications for noble gases in lunar soil grains. Geochim. Cosmochim. Acta 57, 3177–3194.
- Galloway, J.N., 2005. The global nitrogen cycle. In: Schlesinger, W.H. (Ed.), Treatise on Geochemistry, v. 8, Biogeochemistry. Elsevier, Amsterdam, pp. 557–584.
- Giletti, B.J., 1991. Rb and Sr diffusion in alkali feldspars, with implications for cooling histories of rocks. Geochim. Cosmochim. Acta 55, 1331–1343.
- Goldblatt, C., Claire, M.W., Lenton, T.M., Matthews, A.J., Watson, A.J., Zahnle, K.J., 2009. Nitrogen-enhanced greenhouse warming on early Earth. Nat. Geosci. 2,

- 891-896.
- Haendel, D., Mühle, K., Nitzsche, H.-M., Stiehl, G., Wand, U., 1986. Isotopic variations of the fixed nitrogen in metamorphic rocks. Geochim. Cosmochim. Acta 50, 749-758.
- Halama, R., Bebout, G.E., John, T., Scambelluri, M., 2014. Nitrogen recycling in subducted mantel rocks and implications for the global nitrogen cycle, Int. J. Earth Sci.
- Hammer, V.M.F., Beran, A., Endisch, D., Rauch, F., 1996. OH concentration in natural titanites determined by FTIR spectroscopy and nuclear reaction analysis. Eur. J. Mineral, 8, 281-288.
- Higashi, S., 1978. Dioctahedral mica minerals with ammonium ions. Mineral. J. 9, 16–27. Hirschfelder, J.O., Curtiss, C.F., Bird, R.B., 1954. Molecular Theory of Gases and Liquids. Wiley, New York, pp. 1219.
- Holloway, J.M., Dahlgren, R.A., 2002. Nitrogen in rock: Occurrences and biogeochemical implications. Glob. Biogeochem. Cycles 16, 1118. https://doi.org/10.1029/
- Holycross, M.E., Watson, E.B., Richter, F.M., Villeneuve, J., 2018. Diffusive fractionation of Li isotopes in wet, highly silicic melts. Geochem. Perspect. Lett. 6, 39-42.
- Honma, H., Itihara, Y., 1981. Distribution of ammonium in minerals of metamorphic and granitic rocks. Geochim. Cosmochim. Acta 45, 983-988.
- Houlton, B.Z., Morford, S.L., Dahlgren, R.A., 2018. Convergent evidence for widespread rock nitrogen sources in Earth's surface environment. Science 360, 58-62.
- Jeynes, C., Colaux, J.L., 2016. Thin film depth profiling by ion beam analysis. Analyst 141, 5944-5985.
- Johnson, E.A., 2006. Water in nominally anhydrous crustal minerals: speciation, concentration and geologic significance. In: Keppler, H., Smyth, J.R. (Eds.), "Water in Nominally Anhydrous Minerals", Reviews in Mineralogy and Geochemistry. vol. 62. pp. 117-154.
- Johnson, B.W., Goldblatt, C., 2015. The nitrogen budget of Earth. Earth Sci. Rev. 148, 150-173.
- Johnson, B.W., Goldblatt, C., 2017. A secular increase in continental crust nitrogen during the Precambrian, Geochem, Perspect, Lett. 4, 24-28.
- Johnson, B.W., Goldblatt, C., 2018. EarthN: a new Earth system nitrogen model. Geochem. Geophys. Geosyst. https://doi.org/10.1029/2017GC007392.
- Jones, R., Goss, J.P., Pinto, H., Palmer, D.W., 2015. Diffusion of nitrogen in diamond and the formation of A-centres, Diam, Relat, Mater, 53, 35-39.
- Laursen, T., Lanford, W.A., 1978. Hydration of obsidian. Nature 276, 153-156.
- Li, Y., Keppler, H., 2014. Nitrogen speciation in mantle and crustal fluids. Geochim. Cosmochim, Acta 129, 13-32,
- Li, I., Bebout, G.E., Idleman, B.D., 2007. Nitrogen concentration and $\delta^{15} N$ of altered oceanic crust obtained on ODP Legs 129 and 185: insights in to alteration-related nitrogen enrichment and the nitrogen subduction budget. Geochim. Cosmochim. Acta 71, 2344-2360.
- Li, Y., Wiedenbeck, M., Shcheka, S., Keppler, H., 2013. Nitrogen solubility in upper mantle minerals. Earth Planet. Sci. Lett. 377, 311-323.
- Li, Y., Huang, R., Wiedenbeck, M., Keppler, H., 2015. Nitrogen distribution between aqueous fluids and silicate melts. Earth Planet. Sci. Lett. 411, 218-228.
- Maldener, J., Hoesch, A., Langer, K., Rauch, F., 2003. Hydrogen in some natural garnets studied by nuclear reaction analysis and vibrational spectroscopy. Phys. Chem. Miner, 30, 337-344.
- Marty, B., Dauphas, N., 2003. The nitrogen record of crust-mantle interaction and mantle convection from Archean to present. Earth Planet. Sci. Lett. 206, 397-410.
- Mibe, K., Fujii, T., Yasuda, A., 1999. Control of the location of the volcanic front in island arcs by aqueous fluid connectivity in the mantle wedge. Nature 401, 259-262.
- Mikhail, S., Sverjensky, D.A., 2014. Nitrogen speciation in upper mantle fluids and the origin of Earth's nitrogen-rich atmosphere. Nat. Geosci. 7, 816–819. Mikhail, S., Barry, P.H., Sverjensky, D.A., 2017. The relationship between mantle pH and
- the deep nitrogen cycle. Geochim. Cosmochim. Acta 209, 149-160.
- Mitchell, E.C., Fischer, T.P., Hilton, D.R., Hauri, E.H., Shaw, A.M., de Moor, J.M., Sharp, Z.D., Kazahaya, K., 2010. Nitrogen sources and recycling at subduction zones: Insights from the Izu-Bonin-Mariana arc. Geochem. Geophys. Geosyst. 11 (2). https://doi.org/10.1029/2009GC002783.
- Mookherjee, M., Welch, M.D., Le Pollès, L., Redfern, S.A.T., Harlov, D.E., 2005. Ammonium ion behaviour in feldspar: variable-temperature infrared and ²H NMR studies of synthetic buddingtonite, N(D,H)₄AlSi₃O₈. Phys. Chem. Miner. 32, 126–131.
- Müller, T., Watson, E.B., Trail, D., Wiedenbeck, M., Van Orman, J.A., Hauri, E., 2014. Diffusive fractionation of carbon isotopes in y-Fe: experiment, models and implications for early solar system processes. Geochim. Cosmochim. Acta 127, 57-66.
- Mysen, B.O., Fogel, M.L., 2010. Nitrogen and hydrogen isotope compositions and solubility in silicate melts in equilibrium with reduced (N + H)-bearing fluids at high pressure and temperature: effects of melt structure. Am. Mineral. 95, 987-999.
- Mysen, B.O., Yamashita, S., Chertkova, N., 2008. Solubility and solution mechanisms of NOH volatiles in silicate melts at high pressure and temperature - amine groups and $hydrogen\ fugacity.\ Am.\ Mineral.\ 93,\ 1760–1770.$
- Nastasi, M., Mayer, J.W., Hirvonen, J.K., 1996. Ion-solid Interactions: Fundamentals and Applications. Cambridge University Press, Cambridge, U.K. (540 pp.).
- Palya, A.P., Buick, I.S., Bebout, G.E., 2011. Storage and mobility of nitrogen in the continental crust: evidence from partially melted metasedimentary rocks, Mt. Stafford, Australia. Chem. Geol. 281, 211-226.
- Regier, M.E., Hervig, R.L., Myers, M.L., Roggensack, K., Wilson, C.J.N., 2016. Analyzing

- nitrogen in natural and synthetic glass by secondary ion mass spectrometry. Chem. Geol. 447, 27-39.
- Richter, F.M., Davis, A.M., DePaolo, D.J., Watson, E.B., 2003. Isotope fractionation by chemical diffusion between molten basalt and rhyolite. Geochim. Cosmochim. Acta 67, 3905-3923.
- Richter, F.M., Dauphas, N., Teng, F.-Z., 2009. Non-traditional fractionation of non-traditional isotopes: evaporation, chemical diffusion and Soret diffusion. Chem. Geol. 258, 92-103,
- Richter, F.M., Watson, E.B., Chaussidon, M., Mendybaev, R., Ruscitto, D., 2014. Lithium isotope fractionation by diffusion in minerals. Part 1: pyroxenes. Geochim. Cosmochim. Acta 126, 352-370.
- Richter, F.M., Chaussidon, M., Watson, E.B., Mendybaev, R., Homolova, V., 2017. Lithium isotope fractionation by diffusion in minerals; part 2: olivine. Geochim. Cosmochim. Acta 219, 124-142,
- Roskosz, M., Bouhifd, M.A., Jephcoat, A.P., Marty, B., Mysen, B.O., 2013. Nitrogen solubility in molten metal and silicate at high pressure and temperature. Geochim. Cosmochim. Acta 121, 15-28.
- Rossman, G.R., Rauch, F., Livi, R., Tombrello, T.A., Shi, C.R., Zhou, Z.Y., 1988. Nuclear reaction analysis of hydrogen in almandine, pyrope, and spessartite garnets. Neues Jb. Mineral. Monat. 4, 172-178.
- Ruiz Cruz, M.D., Sanz de Galdeano, C., 2008. High-temperature ammonium white mica from the Betic Cordillera (Spain). Am. Mineral. 93, 977-987.
- Ryssel, H., Ruge, I., 1986. Ion Implantation. John Wiley, New York.
- Sadofsky, S.J., Bebout, G.E., 2004. Nitrogen geochemistry of subducting sediments: new results from the Izu-Bonin-Mariana margin and insights regarding global nitrogen subduction. Geochem. Geophys. Geosyst. https://doi.org/10.1029/2003GC000543.
- Shannon, R.D., 1976. Revised effective ionic radii and systematic studies of interatomic distances in halides and chalcogenides. Acta Crystallogr. A32, 751-767.
- Sidey, V., 2016. On the effective ionic radii for ammonium. Acta Crystallogr. B72, 626-633.
- Sio, C.K., Roskosz, M., Dauphas, N., 2018. The isotope effect for Mg-Fe interdiffusion in olivine and its dependence on crystal orientation, composition and temperature Geochim. Cosmochim. Acta 239, 463-480.
- Svensen, H., Bebout, G.E., Kronz, A., Li, L., Planke, S., Chevallier, L., Jamtveit, B., 2008. Nitrogen geochemistry as a tracer of fluid flow in a hydrothermal vent complex in the Karoo Basin, South Africa. Geochim. Cosmochim. Acta 72, 4929–4947.
- Thomas, J.B., Cherniak, D.J., Watson, E.B., 2008. Lattice diffusion and solubility of argon in forsterite, enstatite, quartz and corundum. Chem. Geol. 253, 1-22.
- Trail, D., Cherniak, D.J., Watson, E.B., Harrison, T.M., Weiss, B.P., Szumila, I., 2016. Li zoning in zircon as a potential geospeedometer and peak temperature indicator. Contrib. Mineral. Petrol. 171, 25. https://doi.org/10.1007/s00410-016-1238-8.
- Wang, L., Gong, W., Wang, S., Ewing, R.C., 1999. Comparison of ion-beam irradiation effects in X₂YO₄ compounds. J. Am. Ceram. Soc. 82, 3321-3329.
- Watenphul, A., Wunder, R., Heinrich, W., 2009. High-pressure ammonium-bearing silicates: implications for nitrogen and hydrogen storage in the Earth's mantle. Am. Mineral, 94, 283-292.
- Watenphul, A., Wunder, B., Wirth, R., Heinrich, W., 2010. Ammonium-bearing clinopyroxene: a potential nitrogen reservoir in the Earth's mantle. Chem. Geol. 270, 240-248.
- Watkins, J., DePaolo, D.J., Huber, C., Ryerson, F.J., 2009. Liquid composition-dependence of calcium isotope fractionation during diffusion in molten silicates. Geochim. Cosmochim. Acta 73, 7341-7359.
- Watkins, J., DePaolo, D.J., Ryerson, F.J., Petersen, B.T., 2011. Influence of liquid structure on diffusive isotope separation in molten silicates and aqueous solutions Geochim. Cosmochim. Acta 75, 3103-3118.
- Watson, E.B., Brenan, J.M., 1987. Fluids in the lithosphere. 1. Experimentally-determined wetting characteristics of CO2-H2O fluids and their implications for fluid transport, host-rock physical properties, and fluid inclusion formation. Earth Planet. Sci. Lett. 85, 497-515.
- Watson, E.B., Brenan, J.M., Baker, D.R., 1990. Distribution of fluids in the continental mantle. In: Menzies, M.A. (Ed.), Continental Mantle. Clarendon Press, Oxford, pp.
- Watson, E.B., Cherniak, D.J., Thomas, J.B., Hanchar, J.M., Wirth, R., 2016. Crystal surface integrity and diffusion measurements on Earth and planetary materials. Earth Planet. Sci. Lett. 450, 346-354.
- Watson, H.C., Richter, F.M., Liu, A., Huss, G.R., 2016. Iron and nickel isotope fractionation by diffusion, with applications to iron meteorites. Earth Planet. Sci. Lett. 451, 159-167.
- Weiss, I.M., Muth, C., Drumm, R., Kirchner, H.O.K., 2018. Thermal decomposition of the amino acids glycine, cysteine, aspartic acid, asparagine, glutamic acid, glutamine, arginine and histidine. BMC Biophys. 11, 2.
- Wood, B.J., Blundy, J.D., 1997. A predictive model for rare earth element partitioning between clinopyroxene and anhydrous silicate melt. Contrib. Mineral. Petrol. 129, 166-181.
- Zhang, Y., Stolper, E.M., Wasserburg, G.J., 1991. Diffusion of a multi-species component and its role in oxygen and water transport in silicates. Earth Planet. Sci. Lett. 103, 228-240
- Ziegler, J.F., Biersack, J.P., 2006. The stopping and range of ions in matter. In: Computer